AD_____

Award Number: W81XWH-11-2-0125

TITLE: The Use of Inhibitors of Mechanosensitive Ion Channels as Local Inhibitors of Peripheral Pain.

PRINCIPAL INVESTIGATOR: Frederick Sachs

CONTRACTING ORGANIZATION: State University of New York at Buffalo
Buffalo, NY 14214

REPORT DATE: March 2014

TYPE OF REPORT: Annual

PREPARED FOR: U.S. Army Medical Research and Materiel Command
Fort Detrick, Maryland 21702-5012

REPORT DOCUMENTATION PAGE

Form Approved
OMB No. 0704-0188

1. REPORT DATE	2. REPORT TYPE	3. DATES COVERED
March 2014	Annual	25 February 2013 - 24 February 2014

4. TITLE AND SUBTITLE
The Use of Inhibitors of Mechanosensitive Ion Channels as Local Inhibitors of

Peripheral Pain.

5a. CONTRACT NUMBER

5b. GRANT NUMBER
W81XWH-11-2-0125

5c. PROGRAM ELEMENT NUMBER

6. AUTHOR(S)
Frederick Sachs

5d. PROJECT NUMBER

5e. TASK NUMBER

5f. WORK UNIT NUMBER

7. PERFORMING ORGANIZATION NAME(S) AND ADDRESS(ES)
State University of New York at Buffalo
Buffalo, NY 14214

8. PERFORMING ORGANIZATION REPORT NUMBER

9. SPONSORING / MONITORING AGENCY NAME(S) AND ADDRESS(ES)
U.S. Army Medical Research and Materiel Command
Fort Detrick, Maryland 21702-5012

10. SPONSOR/MONITOR'S ACRONYM(S)

11. SPONSOR/MONITOR'S REPORT NUMBER(S)

12. DISTRIBUTION / AVAILABILITY STATEMENT
Approved for Public Release; Distribution Unlimited

13. SUPPLEMENTARY NOTES

14. ABSTRACT
This is a basic research project designed to understand the role of mechanically sensitive excitatory ion channels (MSC) in the pathology of chronic pain, and the use of a small peptide inhibitor of these channels called GsMTx4 to treatment peripheral pain. The first aim of this project is to understand the mechanism of inhibition of a peptide inhibitor of caution selective mechanosensitive ion channels (MSCs) called GsMTx4 insertion depth in the mutagenisis. In aims 2 and 3 the goals are to understand the gating properties of MSC's, their sensitivity to inflammatory agents and their control by the cytoskeleton. We have shown that GsMTx4 insertion depth in the bilayer is an important factor affecting its inhibitory activity and that the positively charged amino acids are key to this attribute. We have identified that mutations to Piezo channels (putative mechnoreceptors of DRGs) that affect inactivation which is a key regulatory point for inflammatory agents. We have observed that the cytoskeleton of DRG's absorbs greater stress when treated with inflammatory agents and that filamin shows greater sensitivity than action.

15. SUBJECT TERMS- none provided

16. SECURITY CLASSIFICATION OF:			17. LIMITATION OF ABSTRACT	18. NUMBER OF PAGES	19a. NAME OF RESPONSIBLE PERSON
a. REPORT	b. ABSTRACT	c. THIS PAGE			USAMRMC
U	U	U	UU	29	19b. TELEPHONE NUMBER *(include area code)*

Table of Contents

Introduction: The focus of this grant is molecular mechanisms of mechanical transduction in dorsal root ganglia cells (DRGs) that are likely to give rise to the sensation of pain. The first goal was to understand how a specific peptide inhibitor of mechanosensitive ion channels (MSCs) acts to suppress transduction. This involves single channel patch clamp electrophysiology assays and the synthesis of mutant peptides to elaborate the contributions of specific molecular components. A second goal is to extend the single channel patch experiments to whole cell recording where the cytoskeleton is more intact. A third goal is understand how external mechanical stress is distributed in proteins of the cytoskeleton since those mechanics affect the stress in the lipid bilayer where the channels reside. Finally, if we arrive at some promising therapies based on *in vitro* data we will measure the analgesic effects of the peptides in intact mice or rats and correlate nociceptive sensitivity.

Body:

Aim 1) GsMTx4 Mechanism of Inhibition

MSC Inhibition by GsMTx4 Mutants:

GsMTx4 is a peptide inhibitor of MSCs that may be useful as a peripheral analgesic. The goal of this aim is to understand the mechanism of inhibition by determining the amino acids important to GsMTx4 interactions with MSCs and the membrane. The long term goal is to use this information to selectively modifying its structure to change its affinity for different targets. A relatively unique feature of GsMTx4 is its high positive charge, which we suspect is important to the peptides mechanism of action. So we constructed 6 lysine to glutamate mutants and measured changes in their inhibition strength on exogenously expressed Piezo 1 channels in outside-out patches from HEK cells (Fig. 1).

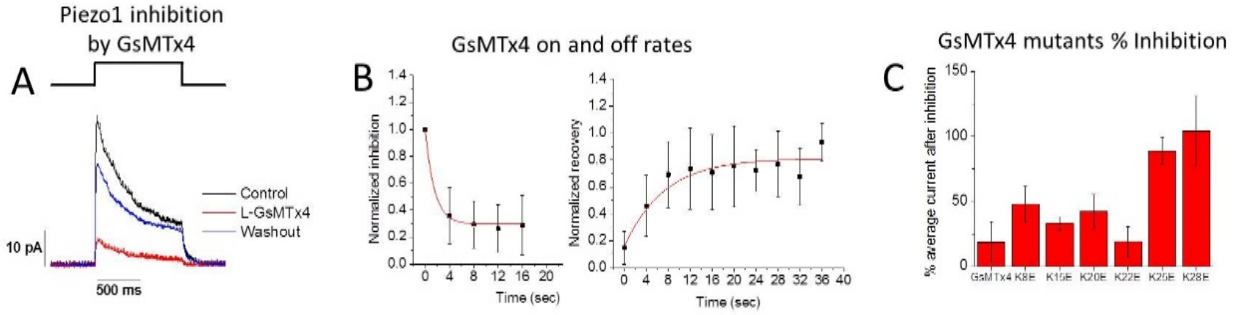

Figure 1. Inhibitory activity of WT, and six K to E mutants of GsMTx4. (A) Shows the average MSC currents from Piezo1 channels before, during and after washout of WT GsMTx4. (B) Shows association and dissociation rates of WT GsMTx4 inhibition. Exponential fits to these data were used to calculate K_Ds for the different peptides. (C) Shows the percent inhibition of Piezo1 patch currents by 5 µM WT and mutant GsMTx4 peptides. The maximal control current before peptide application for each set of data was 100%. K25E and K28E show almost complete loss of inhibition.

Simulation of GsMTx4 Bilayer Association:

At the time of our last yearly report, we were near to the conclusion that lysine mutants that had the greatest loss of inhibitory activity also bound at shallower depths in the bilayer. Molecular dynamics

simulations of GsMTx4 binding to lipid bilayers performed by Dr. Kazu Nishizawa's laboratory at Teikyo University showed that the wt peptide enters a deep binding mode. Mutations that disrupted inhibition of the Piezo channels to the greatest degree were the ones that showed the shallowest bilayer depths in the Dr. Nishazawa's simulations (Fig. 2). If inhibition strength is dependent on depth penetration in the bilayer we thought it would be possible to test this model in lipid based binding assays. So we contacted two collaborators who had assays capable of determining peptide-lipid binding strength and penetration depth.

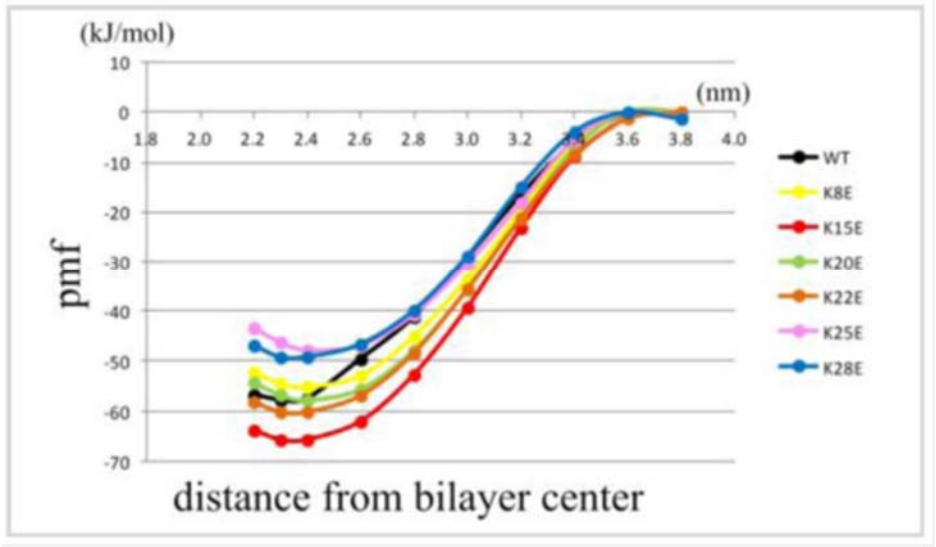

Figure 2. Coarse grain simulations shows potential mean force necessary to maintain positions of wt and mutant peptides at varying depths within a bilayer. The distances from the membrane center are shown on the x-axis. The peak negative values at 2.4 nm above the membrane center shows that these peptides are most stable residing at the bilayer lipid-water interface. However, K25E and K28E (mutants with greatest loss of inhibition) have the lowest stability (least negative ΔG) at 2.4 nm depth.

GsMTx4 Lipid Binding Studies:

Dr. Sergei Sukharev of the University of Maryland and Dr. Alexey Ladokhin performed a number of physiochemical experiments on the WT and mutant peptides to show structural and lipid binding properties. Circular dichroism spectrum showed that all KtoE mutant peptides had a distinct negative peak at ~227 nm (Fig. 3A). This peak disappeared and the spectrum were nearly indistinguishable from WT when the mutant peptides were allowed to bind lipids, suggesting peptide folding was not affected by the mutations. However, the peaks did suggest that aggregation of the peptide was occurring in solution which could affect binding. We determined the state of aggregation by dynamic light scattering (Fig. 3B) and by peptide migration on non-denaturing gels (Fig. 3C). We observed 80-160 nm aggregates for WT and mutant peptides at 30 µM. Most mutant peptides showed larger aggregates than WT. In order to determine if aggregation was significant at concentrations near the K_D of the peptide, we ran them at different concentrations on nondenaturing gels. While larger migrating complexes were observed above 10 µM, little aggregation was observed at 3 µM. Also there was no differences in the

size of the aggregates for either WT or the mutants, suggesting that aggregation is not a significant factor affecting the mutant peptide inhibitory differences.

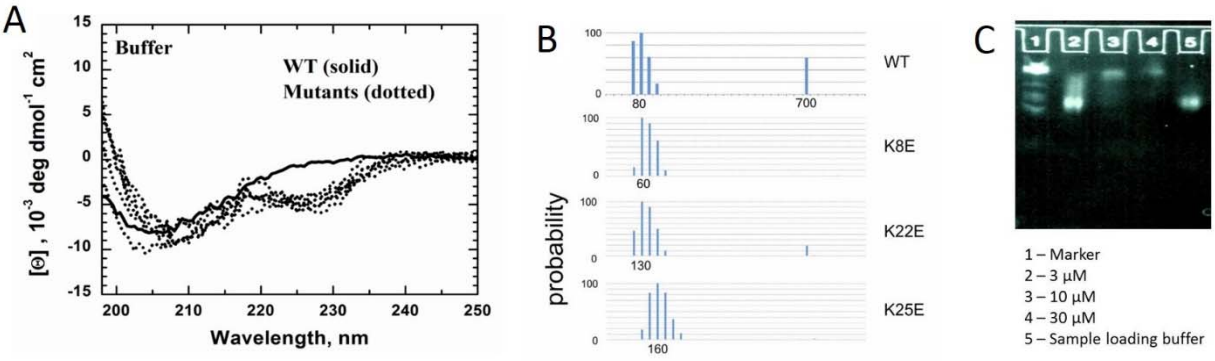

Figure 3. (A) Circular Dichroism spectrums of wt and KtoE mutants of GsMTx4 shows mutants all have a distinct negative peak centered at ~227 nm. This peak disappears when the peptides are associated with lipid vesicles. (B) WT and mutant GSMTx4 peptide was dissolved at concentrations of 30 µM and light scattering was measured. Histograms showing the average size aggregates in nm show different aggregation sizes for the mutants compared to WT. (B) Three concentrations of GsMTx4 (3 µM, 10 µM, 30 µM) and sample loading buffer alone were run on a 10-20% Tris-Tricine polyacrylamide gel. Both the sample loading buffer lane and the 3 µM GsMTx4 lane migrated further than the two lanes loaded with higher concentrations of GsMTx4. Streaking was apparent even in the lane with the lowest concentration of GsMTx4, suggesting some aggregation is occurring even at 3 µM.

We applied the WT and mutant GsMTx4 peptides to monolayers in a Langmuir-Blodgett trough and measured the pressure vs area (Fig. 4A), and pressure vs surface potential (Fig. 4B) isotherms. As a point of reference we used the monolayer-bilayer equivalence pressure (MBEP) which occurs at ~40 mN/m. In both experiments it was obvious that the WT and mutant peptides had strong attractions to the air-water-lipid interface since, even at low areas when the monolayer was in a disordered state, significant pressure increases were observed. For the PA isotherms, greater areas observed at a particular pressure suggests stronger affinity of the test molecule to the interface. Most mutants showed subtle variations in the area at the MBEP compared to WT peptide, though K25E and K28E were noteworthy in that they showed the greatest deviations (-5 and +15 $Å^2$ respectively, Fig. 4A). Monolayers in the presence of K25E were nearly equivalent to untreated monolayers at the MBEP suggesting complete dissociation of the peptide at this pressure.

The mutants also showed subtle differences in their contribution to surface potential compared to WT (Fig. 4B). These difference likely reflect the contribution of the test molecule to lipid packing and structuring water molecules at the interface. Lower potentials at the MBEP can mean increased disorder of the monlayer-water interface and represent lower stability of the monolayer at that pressure. It is unclear how this relates to the peptide interaction with the interface, though lower surface potential may represent greater disorder of the bilayer surrounding the channel which could affect tension transmission. In Figure 4B, WT GsMTx4 shows a subtle decrease in the surface potential compared to untreated membranes. We are currently testing this hypothesis with higher peptide concentrations.

We also allowed the peptides to bind to vesicles in solution containing iodine to quench the tryptophan fluorescence (Fig. 5A). GsMTx4 has two adjacent tryptophans (W6 and W7) that make up a substantial

fraction of the peptide hydrophobic face, likely oriented toward the interior of the membrane. These tryptophans would have less exposure to the buffer for deeper binding mutants. Here we see that, although the ΔG (concentration dependence of association) of K25E and K28E binding are similar, K28E tryptophans are significantly less exposed (deeper binding) than WT peptide, while the tryptophans on K25E are more exposed (possibly shallower depth). The deeper binding depth of K28E was confirmed by using brominated lipid quenching of the tryptophans (Fig. 5B). K28E shows significantly greater quenching by bromine at different depths within the bilayer than WT, suggesting deeper penetration.

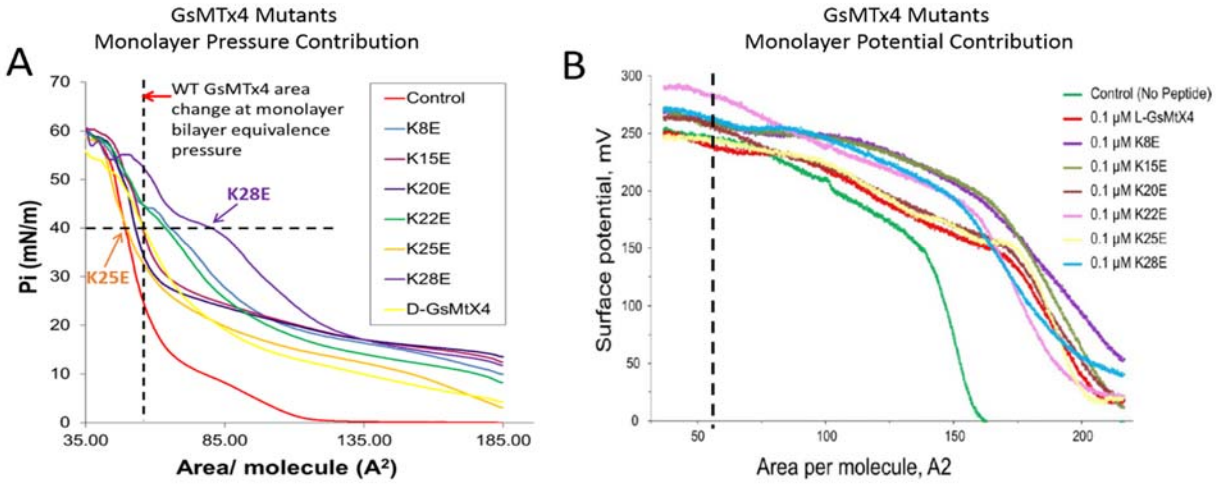

Figure 4. GsMTx4 and mutant effects on lipid monolayer area and surface potential as a function of pressure. (A) WT and lysine mutants of GsMTx4 (1 µM) were added to 3:1 POPG:POPC monolayers in a Langmuir-Blodgett trough and allowed to bind the surface in the disordered state. The pressure on the monolayer was increased (area decreased) until it disrupted and the pressure vs area isotherm records are shown. Greater increase in area with pressure indicates the peptide is occupying more area in the monolayer and likely to have deeper intercalation and higher affinity. The two mutants of GsMTx4 with the greatest loss on inhibitory activity (K25E and K28E) are the greatest outliers from WT area occupancy. (B) The same peptides were tested at 0.1 µM while measuring surface potential on the monolayer. WT GsMTx4 produces a subtle decrease in surface potential at the MBEP suggesting a disordering effect on the monolayer.

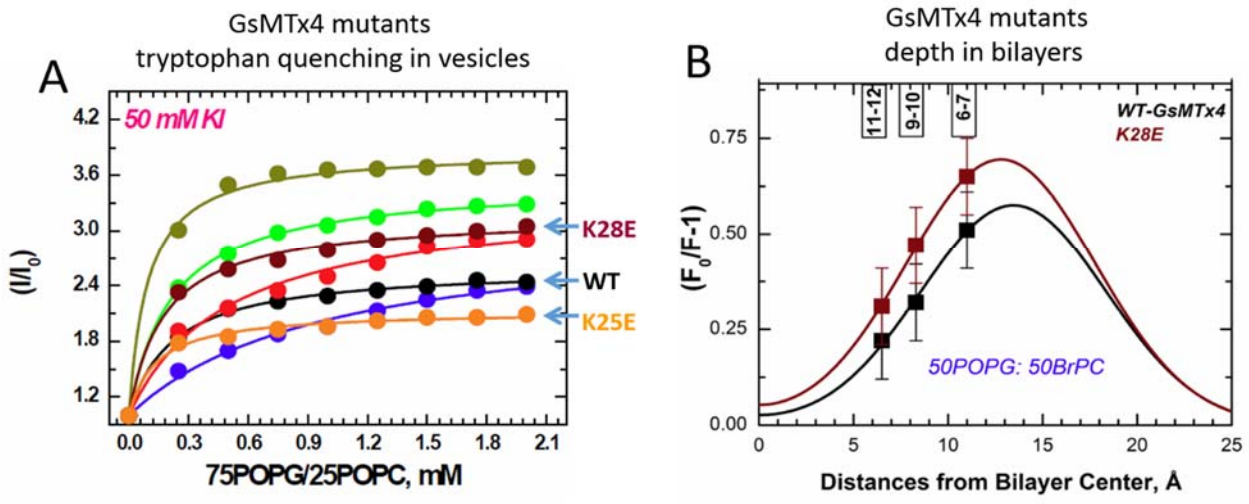

Figure 5 (A) Binding affinity of WT and lysine mutants to 3:1 POPG:POPC membranes inhibits tryptophan quenching by Iodine in solution. Greater penetration of the peptide usually leads to greater protection and reduced quench. K25E is quenched

more than WT and K28E is quenched less. (B) WT and K28E mutant peptide were allowed to bind to 1:1 POPG:BrPC vesicles and the percent of quenching was determined. Bromine atoms which quench tryptophan fluorescence were located on the acyl chain of the POPC at different carbons (positions are shown at the top of the graph). At each depth the K28E mutant peptide was clearly quenched to a greater extent suggesting deeper penetration depth in the bilayer.

These data could be interpreted as showing that GsMTx4 inhibitory activity arises from the peptides interfacial binding depth which is at an ideal depth for the WT form. Deeper or shallower occupancies decreases its effectiveness. There is some evidence for this hypothesis in a recent modeling study that simulated GsMTx4 and HpTx2, a related peptide, binding to bilayers [1]. In this study GsMTx4 had a more negative ΔG for binding, but did not bind as deep as HpTx2. GsMTx4 had strong tendency to straddle the interfacial region and created significantly greater far field thinning of the membrane which is attributed to its high electrostatic charge. The far field thinning appeared sensitive to binding depth. This is in agreement with the K25E and K28E data. Further studies with different lipid compositions to probe binding to raft like membranes, brominated lipid quenching and new mutants to the hydrophobic region will be key to confirming these results and identifying potential sites of interaction on biological membranes.

Work to be completed in extension period:

We have requested a no cost extension for 6 months to complete the goals of the aims. For Aim 1 we need to complete 3 objectives to publish the results of GsMTx4 lysine mutant studies:

1) Test 2 more mutants in the vesicles containing Bromine at different depths.
2) Determine concentration dependence of GsMTx4 inhibition of Piezo 1. We already have 2 concentrations complete and need 3 more concentration points to curve fit the relationship. This kinetics of the relationship will give us a measure of the peptide cooperativity and of the number of peptides/channel required for block.
3) Run 2 more mutants on non-denaturing gels.

Aim 2) MSC Gating Properties and Sensitivity to Inflammatory Reagents

The goals of this aim are to study the gating kinetics of MSCs in both the patch and in whole cell currents from isolated differentiated DRG neurons and from HEK cells expressing exogenous putative MSCs. To do this we are incorporating a variety of techniques to mechanically stimulate cells and to measure the channel activity. We are also creating mutations to investigate the inactivation properties of MSCs which has been shown to be a major contributor to neuronal sensitivity to mechanical stimulation [2]. We are also working to identify the MSC protein subunits in DRGs involved in the inflammatory response and to investigate how their gating properties are affected by inflammatory mediators.

Piezo channel inactivation:

The role of PIEZO1 inactivation is critical to the function of the PIEZO channels. This is evident from recent work that has shown that mutations that affect the kinetics of inactivation (slower inactivation) are associated with disease states such as Xerocytosis (Stomatocytosis) [3, 4] for PIEZO1 and

Arthrogryposis (PIEZO2) [5]. In the case of DRGs currents that are elicited by a stimulus the inactivation rates can vary. Recently, the Lewin group showed that these currents may come from PIEZO2 channels whose response is modified by proteins (STOML3) tuning the response of the channel [6].

We have examined inactivation of PIEZO1 using two mutations M2225R and R2456K (called DhPIEZO1) that completely removes inactivation [7]. The loss of inactivation was accompanied by ~30 mmHg shift of the activation curve to lower pressures and slower rates of deactivation. The slope sensitivity of gating was the same for WT and mutants indicating that the dimensional changes between the closed and open state are unaffected by the mutations. These are not associated with pore since the unitary channel conductance was unchanged. DhPIEZO1 was reversibly inhibited by the peptide GsMTx4 that acted as a gating modifier. The channel kinetics were solved using complex stimulus waveforms and the data fit to a three state loop in detailed balance. The reaction had two pressure dependent rates, *closed* to *open*, and *inactivated* to *closed*. Pressure sensitivity of the opening rate with no sensitivity of the closing rate means that the energy barrier between them is located near the open state. Mutant-cycle-analysis of inactivation showed that the two sites interacted strongly, even though they are postulated to be on opposite sides of the membrane. A key observation is that even in whole cell recordings the PIEZO channel does not inactivate indicating that there is no contribution to channel inactivation by adaptive response of the cell.

Piezo channel domain structure:

We are able to split the PIEZO channel and reassemble the two segments into an active channel. We discovered this serendipitously when trying to covalently link the PIEZO protein with a fluorescent GFP protein. The resulting channel kinetics were unlike the wild type - they did not inactivate (Fig. 6). We were interested in working with a channel that had wild type kinetics and we began to introduce probes internally to the channel sequence and found that inserting the fluorescent protein mCherry at position 1591 produced a fully functional channel (Fig. 6).

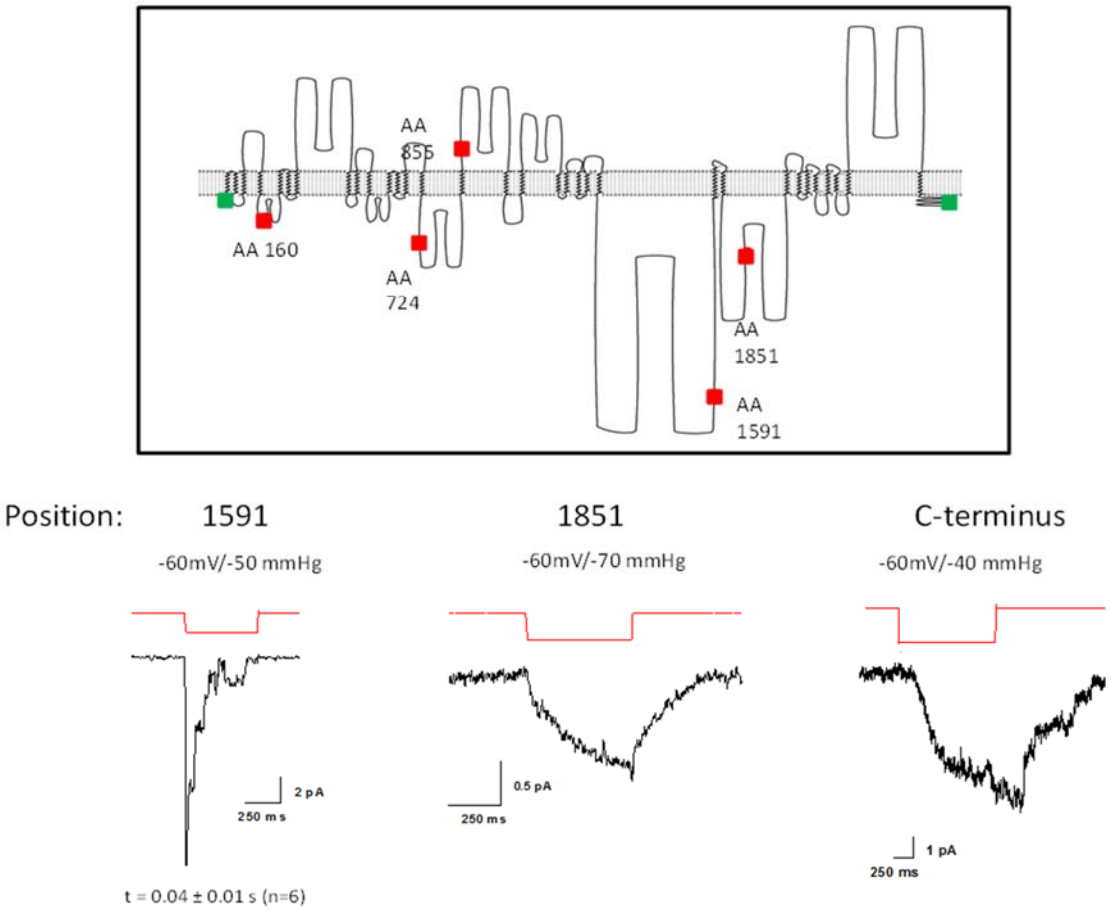

Figure 6 PIEZO1 with an internal mCherry behaves like the wild type channel. To create a fluorescent GFP-PIEZO1 we first attached it to the C or N termini. These channels did not inactivate (bottom trace -Right). We then introduced mCherry into an internal loop at the indicated positions and found no response from channels labeled at positions 160, 724 and 855, but at position 1591 (called 1591-mCherry-PIEZO1-Left). PIEZO1 with an insertion at position 1851 had low current and did not inactivate.

An important use of this fluorescent construct is to image the channels in cells especially when mutations are made to the channel. We imaged the PIEZO1 protein distributed in HEK293 cells using Structured Illumination Microscopy. Figure 7 shows the image of a cell that was cotransfected with 1591-mCherry-PIEZO1 and TREK-GFP, both mechanical channels, although TREK is K^+ selective. The image was reconstructed into a 3-D image from a Z stack of 24 images. The large red clusters are PIEZO1 channels. Notice that there is no significant spatial overlap between the two types of channels so they are likely in different mechanical domains that likely have different stresses. The mechanical responses of the cells could span a wide range of stimulus magnitudes regardless of the intrinsic channel gating properties as they are presumably located in cellular domains of different stress.

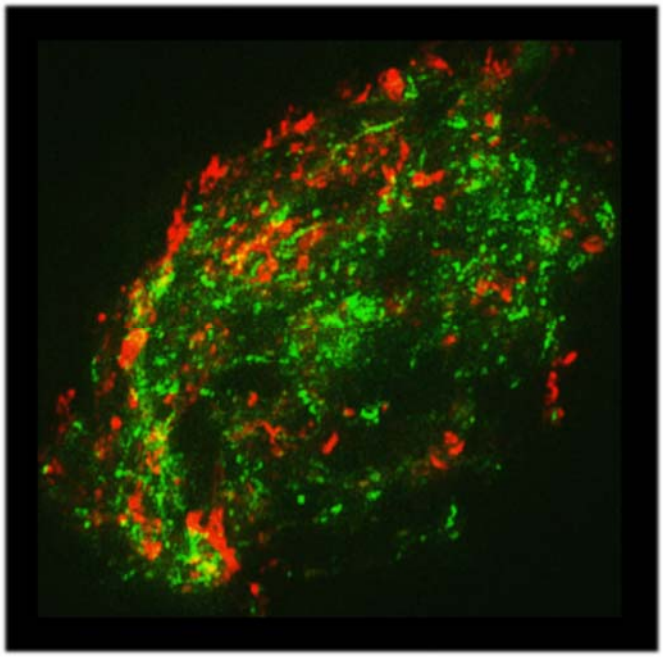

Figure 7 PIEZO1 channels form clusters and TREK-1 is more widely distributed. PIEZO1 (red) and TREK1 (green) are located on the surface of HEK cells. PIEZO1 is tagged with internal mCherry and TREK-1 is linked at its C-terminus to GFP. Cells were transfected and after 24 hours fixed with 4% paraformaldehyde. Data were collected by Structured Illumination Microscopy (24 level z-stack) and reconstructed into a 3D model using ImageJ. TREK-1 forms bead like domains that appear to follow the underlying cytoskeleton. In contrast, PIEZO1 forms large clusters domains. There is no significant spatial overlap between the two types of channels.

Next we split the sequence at the mCherry site and made a vector that expressed both the N- and C-terminal fragments separately but simultaneously (fragments 1-1591 and 1592 -2521). To allow us to monitor expression, the N-terminal fragment was labeled with mCherry at its C-terminal and the C-terminal fragment was labeled with GFP at its N-terminal (Fig. 8). We then expressed both components in cells and measured the responses in whole-cell and cell-attached modes. The two independent parts of the expressed channel clearly reassembled into a functional unit with kinetics similar to the wild type (Fig. 9). Notice that inactivation normally slows with depolarization. We have tested each fragment individually and we were unable to generate whole-cell or patch currents. This argues that there are some elements in each fragment are needed to reconstitute a functional channel or that the channel requires elements to be transported to the plasma membrane.

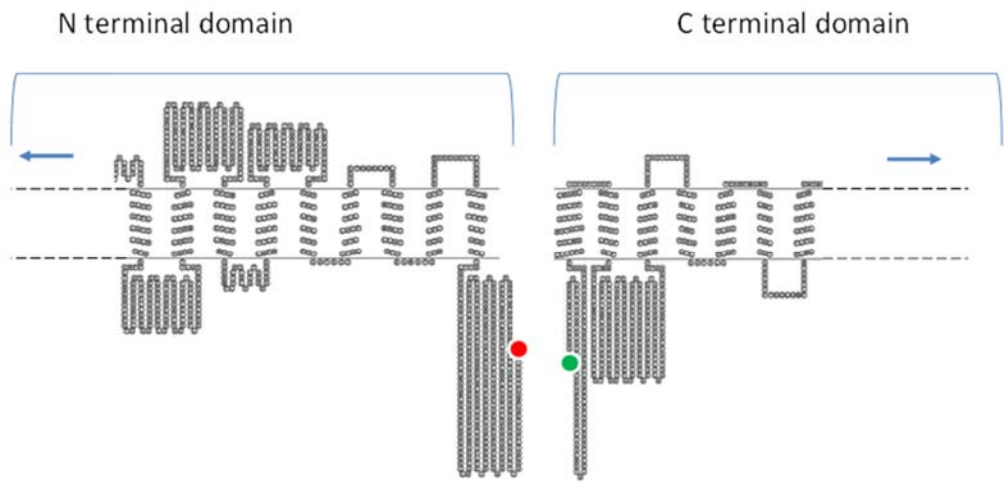

Figure 8 Two PIEZO1 fragments when coexpressed produced an active channel. This construct allows access to internal transmembrane domains where we can delete sequences to produce smaller channels. Fluorescent tags are indicated by colored circles.

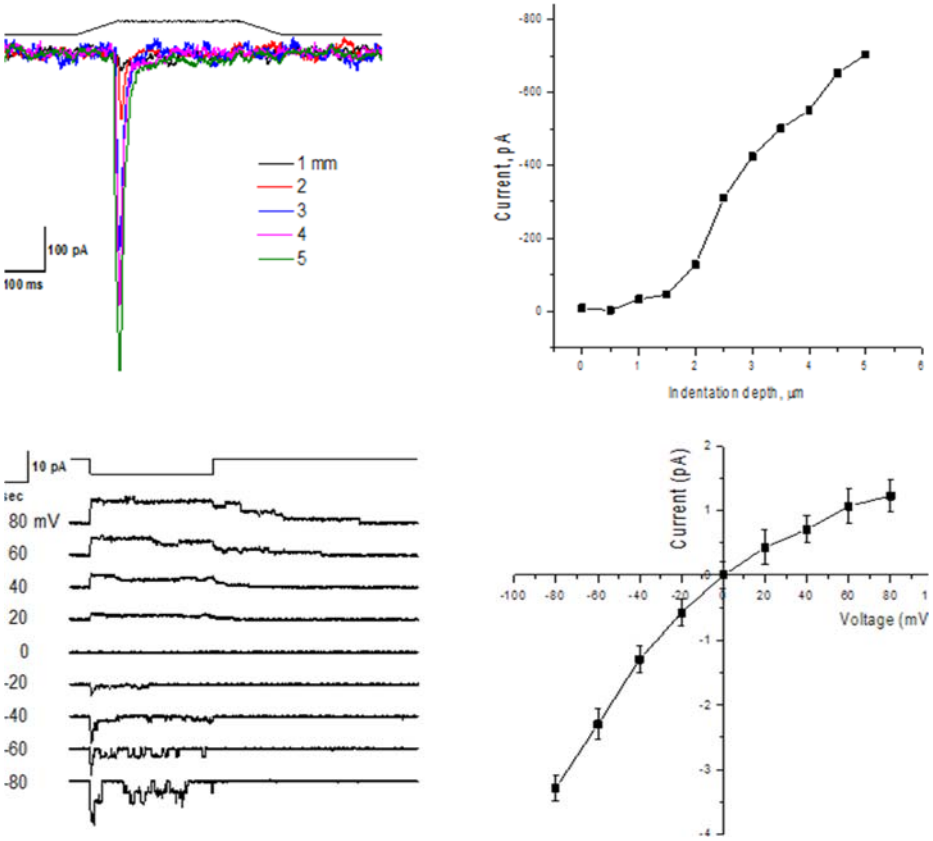

Figure 9 Reassembly of PIEZO1 fragments into a functional channel. The plasmid created expression of two independent protein segments in HEK293T cells. Cells were identified by both green and red fluorescence. Panel A shows whole cell currents elicited by indenting the cell with a fire polished probe at a holding potential of -60 mV. Panel B is a dose-response curve of mechanical sensitivity with increasing depths of penetration producing more current. Panel C is a recording of single channel currents from a cell-attached patch at the indicated voltages showing inactivation with depolarization. This

emphasizes that the channels couple mechanical stress to membrane potential in time dependent ways. Panel D is an IV curve derived from the cell-attached single channel traces.

DRG MSCs sensitivity to inflammatory agents:

We have observed that treatment of DRG neurons with inflammatory agents affect indentation induced phasic currents (Fig. 10). Similar to that reported for Piezo 2 channels after Bradykinin treatment, we see an increase in current amplitude and slowing of the inactivation/adaptation rates. There are currently no reports showing modulation of MS currents as a result of changes in slope sensitivity to membrane tension, suggesting the intrinsic tension sensing structures are not likely significant points of regulation. Regulation of MSC activity most likely occurs by controlling the tension that reaches the channels and by modification of inactivation properties, typically slowing. Both these properties appear to be under the control of the local cytoskeleton, and actin and tubulin networks may both be involved.

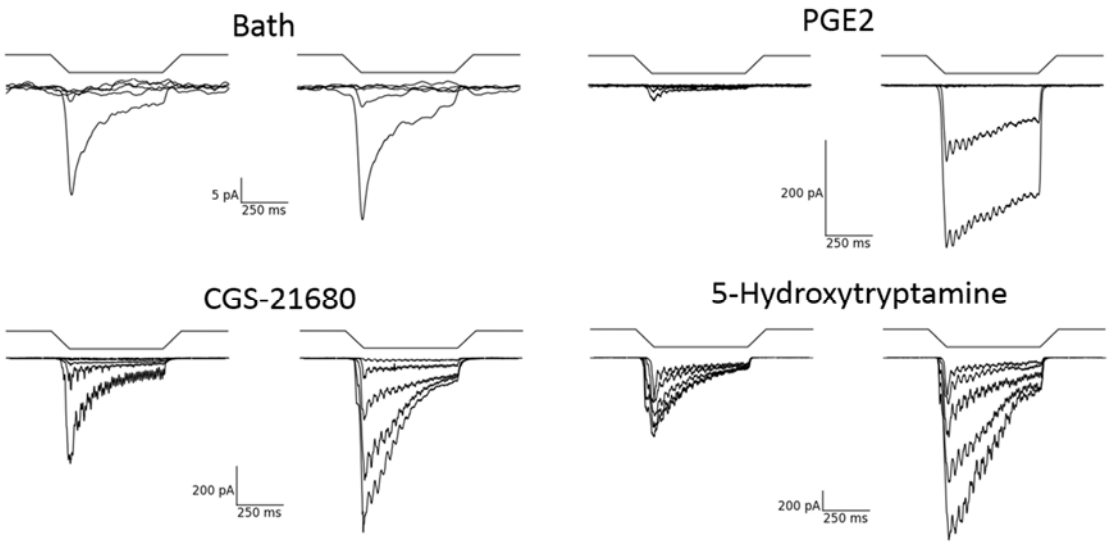

Agent tested	Δτ (increase or decrease)	fold increase in current
Bath	-25 ms	0.22
5-HT	328 ms	1.3
CGS	153 ms	1.6
PGE2	592 ms	10

Figure 10 Inflammatory agents increase the amplitude and slow inactivation of MS currents in DRG neurons. Voltage-clamped DRG neurons were mechanically indented to 5 depths from 6-10 µm with a fire polished glass probe to elicit MS currents. The mean MS currents at each depth from 5-6 cells were averaged to produce the ensemble currents shown.

Recordings on the left show the average control MS currents before treatment, while traces to the right show currents 4-8 min after perfusion with new saline alone (Bath), or saline containing inflammatory agents (100 µM 5-HT or PGE2) or an adenosine A2A GPCR agonist (100 µM CGS-21680). CGS-21680 agonist mimics many of the inflammatory agents by activating cAMP dependent pathways. The time constants determined by exponential fits to the decaying current of the largest responses before and after treatment are shown with the peak amplitudes in the table below. Only neurons that produced MS currents without treatment were used for testing. Differences in the amplitude and inactivation rates of the initial currents among the four groups represents the heterogeneity of the DRGs selected from the cultured neurons. Mechanically perturbing the DRGs with saline changes alone (Bath -control) produced no change in the inactivation properties or amplitude of the MS currents. When inflammatory mediators (100uM 5-HT or PGE2) or CGS-21680 were added to the saline change there was a significant increase in current amplitude and slowing of inactivation.

Fluorescence detection of Membrane Voltage:

An impediment to efficiently determining the sensitvity of MS currents to different inflammatory agents is that we are limited to one neuron per dish when performing electrophysiology recordings due to the length of recordings and treatment contamination of other cells. In order to increase the number of DRGs tested per coverslip we have incorporated the use of the membrane voltage sensitive fluorescent dye di-8-ANEPPS to measure MS currents. Di-8-ANEPPS and other environmentally sensitive dyes have been used for many years to measure neuronal currents, and this technology has recently been used to monitor whole cell currents with sub millisecond resolution [8]. It is non-invasive and multiple cells per coverslip can be tested since we are not tethered to the position of the electrode. Preliminary data demonstrates that we are able to observe MS currents electrically and fluorecently simultaneously (Fig. 11). The signal strength is currently weak (2% change in ratio for 100 mV change), but can be significantly improved (>10% for 100 mV change) with optimal filters for the ratio measurement (optimal filters 560 and 620 nm).

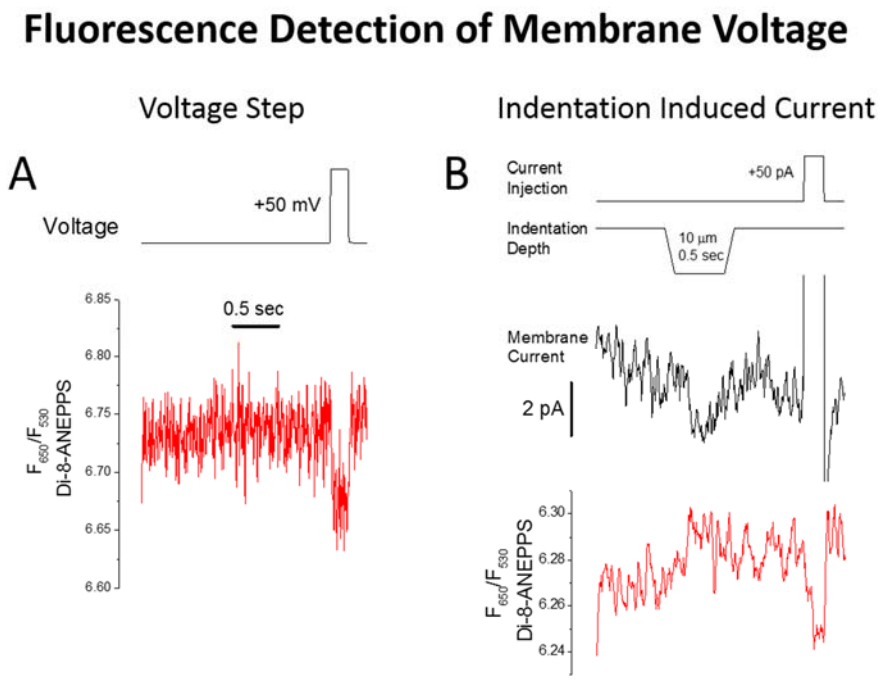

Figure 11 DRG neurons were loaded with di-8-ANEPPS for 10 min and washed for 10 min. A dye loaded cell was whole-cell voltage clamped and imaged were acquired at 200 Hz at both 530 and 650 nm using a Dualview splitter for ratiometric analysis. The optimal wavelengths for (A) In voltage clamp mode the we applied a +50 mV voltage step to the neuron and the fluorescent ratio measurement accurately follows the step with 5 ms resolution. However, <1 ms resolution can be achieved

once filter sets are optimized. (B) In current clamp mode, an indentation of the cell with the glass probe elicited a small current influx that was detected in the ratio signal.

DRG MSC sensitivity to inhibitors:

Four types of mechanoreceptor currents have been identified based on the rate of the decay of the phasic (inactivation/adaptation) response [2]. There are rapidly adapting (RA - ~3-6 ms), intermediate adapting (IA - ~15-30 ms), slowly adapting (SA – ~200-300 ms) and ultra-slowly adapting (uSA - ~1000 ms) currents generated by pressing on peripheral afferents. It has been proposed that neurons expressing the RA currents would provide better spatial and temporal resolution and are likely involved in light touch sensitivity, while the SA type currents are more closely associated with nociception. Although the current associated with the two main types of pain are not restricted to a specific type, modulation of neurons with RA currents is more commonly linked to allodynia, while hyperalgesia more likely emanates from SA type cells. Although different reports have suggested involvement of multiple channel types as potential mechanotransducers in somatosensory neurons, TRPA1, TRPV4 and Piezo 2 have emerged as leading candidates.

We have expressed Piezo 2 channels in HEK cells and observed rapidly inactivating currents in both outside-out patches (Fig. 12A and B) and whole-cell indentation currents that are blocked by GsMTx4 (Fig. 12C). However, GsMTx4 appears to have little effect on HC030031 sensitive SA currents (Fig. 12D) which are likely produced by TRPA1. Thus GsMTx4 may selectively inhibit RA currents though further experiments on specific DRG subtypes will be required.

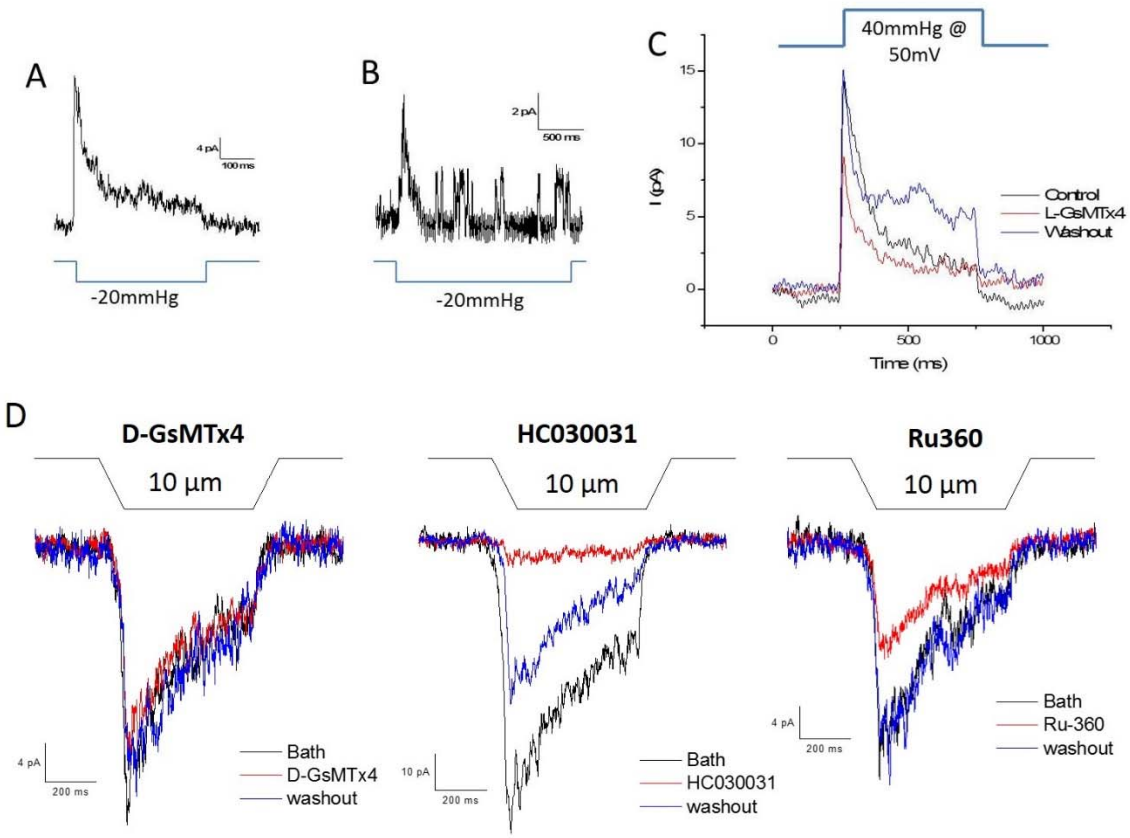

Figure 12 GsMTx4 blocks Piezo 2 currents expressed in HEK cells, but not slowly adapting currents in DRGs. A Piezo 2 pIRES vector was expressed in HEK cells so that GFP was an indicator of expression. (A) Shows rapidly inactivating average current

from a cell-attached patch from a green fluorescent cell. (B) Individual trace showing inactivation of single channels. (C) Average currents from an outside-out patch from a Piezo 2 expressing cell is >50% inhibited by 5 µM GsMTx4. (D) SA currents induced by indentation from a cultured DRG. All three recordings are from a single cell with each record representing the average current from 5 indentations before, during and after application of different inhibitors. Three compounds were tested: GsMTx4 – 24% inhibition, HC030031 (TRPA1 inhibitor) – 94% inhibition, and Ru360 (TRRP V and C blocker) – 47% inhibition.

The evidence of MSC sensitivity to inflammatory agents is nearly complete and will be the first report of sensitivity to these specific agents. The last piece of data needed is to determine the sensitivity of the different whole cell currents (rapid, intermediate and slowly adapting) to different inhibitors such as GsMTx4, HC030031 and Ruthenium Red to provide an assessment of the channels involved. The changes in channel properties will be presented together in a report with the cytoskeletal data in Aim 3 which demonstrates that the changes in channel properties may be linked to modification of cytoskeletal distribution.

Aim 3) Cytoskeletal Membrane Tension Control in DRGs

In this aim we are investigating the stress distribution on different cytoskeletal proteins in DRGs using the FRET based stress reporting probes we have developed. Constitutive stress levels in the cell body and neurites will be measured and changes in stress after treatment with inflammatory agents. We will also induce macroscopic stress in the DRGs with probe pressure in different regions of the cell and monitor the currents and the GsMTx4 sensitive Ca^{2+} influx.

Actinin and Filamin sensitivity to inflammatory agents:

The cytoskeleton can control MSCs on multiple levels. The cytoskeleton is responsible for controlling bilayer stress and the localization of membrane proteins in lipid domains, or near adapter proteins. Stresses in the cytoskeleton are complicated by their three dimensional distribution and non-uniformity. Identifying the specific cytoskeletal elements responsible for controlling bilayer stress has been hampered by the lack of tools to study cytoskeletal stresses in individual elements. Using our FRET based stress sensing protein cassette called cpstFRET we have characterized the resting and dynamic responses of filamin and actinin chimeras in DRG neurons when treated with inflammatory agents (Figs. 9 and 10).

Although actinin and filamin have similar affinities for actin, they modulate the stiffness of actin networks differently because they crosslink fibers in different orientations. . Filamin has a pronounced role in crosslinking the actin network to other membrane proteins and has been implicated in regulating membrane signaling complexes in a stress-dependent manner, including modifying MSC gating.

In the resting cells stresss response (Fig. 13), control experiments examined the effect of simply exchanging the saline, and we observed a change in tension. Interestingly, actinin consistently showed a transient increase in stress while filamin showed a prolonged decrease in stress. These responses were likely caused by minor osmolarity changes or shear stress from the fluid movement. Neither chimera showed significant changes in resting tension from 5-HT exposure. Both showed an increase in stress in response to cAMP induction by CGS-21680, but only actinin had a strong increase in response to PGE2.

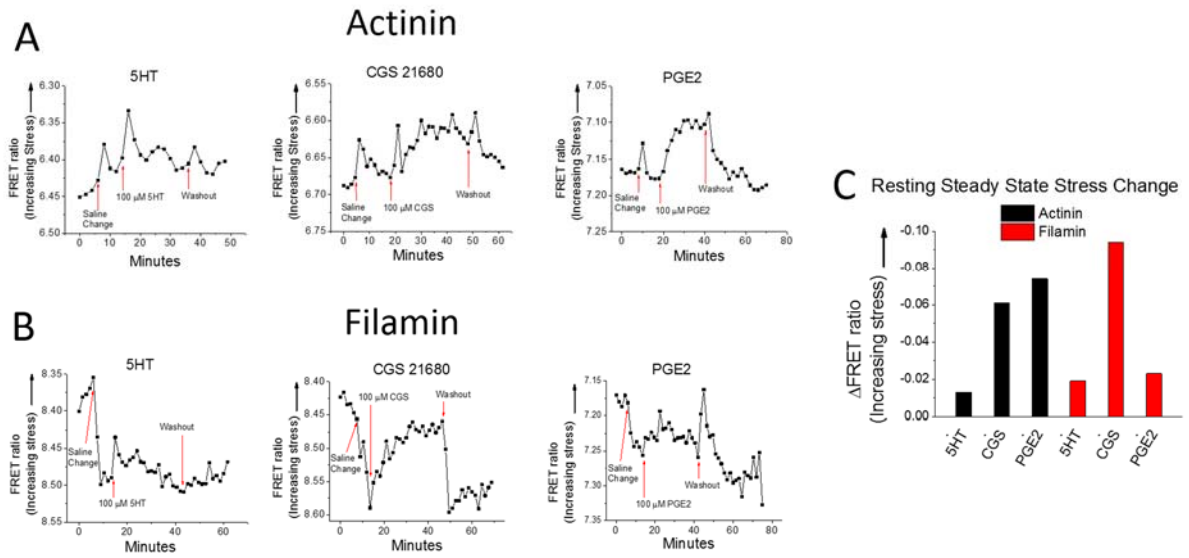

Figure 13. Inflammatory Agents Cause Resting Stress Changes. The resting FRET ratio was monitored for cpstFRET-actinin (A) and cpstFRET-filamin (B) chimeras expressed in DRG neurons. Each trace shows the average response from 15-20 neurons. The cells were challenged with a saline change alone, followed by a saline change including 100 µm of an inflammatory agent indicated by the red arrows. After 20-30 minutes of treatment the inflammatory agent was washed out. 5HT - serotonin, CGS 21680 - adenosine A2A receptor agonist, PGE2 - prostaglandin E2. Saline changes alone mechanically disturb cells probably by fluid shear stress and/or possibly by subtle osmotic changes. Actinin showed a transient stress increase, while filamin showed a sustained decrease in stress in response to saline changes. Cells also show sustained differential sensitivity to the three inflammatory agents. The mean stress changes after 10-15 min treatment with the inflammatory agents is shown in (C). 5HT induces a small change in stress, CGS 21680 induces a large changes in both cytoskeletal elements, and PGE2 selectively induces a large change only in actinin.

We also examined dynamic stress changes in cells expressing the two chimeras by indenting the soma of neurons to a depth that normally elicited MS currents in electrophysiology recordings (Fig. 14). Again both chimeras showed weak sensitivity to 5-HT treatment (no change from control response), but strong stress increase in response to PGE2 treatment. Only filamin showed a response CGS-21680.

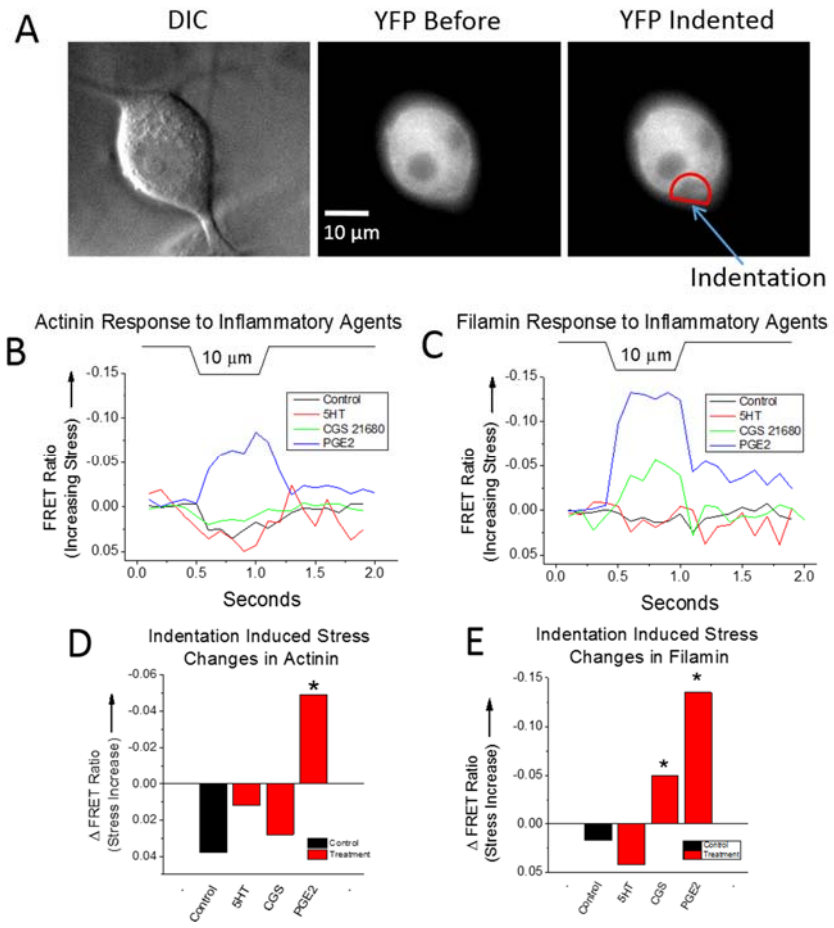

Figure 14. Inflammatory agents cause changes in the cytoskeleton sensitivity to stress. DRGs transfected with cpstFRET chimeras of actinin and filamin were indented with a blunt glass probe – tip ~3-4 µm diameter. The cell were indented ~10 µm with a trapezoidal shaped 0.5 sec long stimulus, a depth that produced maximal MSC currents in whole-cell recordings. (A) Shows a DIC image of a DRG soma, and the YFP fluorescence images before and at the peak of the indentation to show the change in distribution of the stress probe. The red semicircle outlines the region of the interest (ROI) used to analyze the FRET changes during indentation. Cells were indented 9 times before and during treatment with inflammatory agents, and the signals averaged. Images were acquired at a rate of 10 frames/sec. The mean response from 15-20 cells was averaged in the ensemble responses shown in (B and C). The FRET response was measured before (black control traces) and after 20-60 min in the presence of inflammatory mediators. Both cytoskeletal elements responded with a small decrease in stress during control indentations (D and E). Treatment with 5HT produced little change in the stress response. CGS 21680 selectively induced stress sensitivity in filamin. PGE2 treatment caused both actinin and filamin to show a robust increase in stress to indentations.

The filamin results are intriguing in light of the role this protein plays in cellular remodeling. Filamin and talin (another cortical adapter protein) compete for binding integrins. Talin association with integrins tends to stabilize long lasting focal adhesion complexes. Filamin tends to destabilize integrin association with the extracellular matrix for cortical remodeling and cell motility. Thus, the internal cytoskeleton bears the majority of cortical stress when filamin-integrin associations are dominant. Thus greater membrane compliance is a likely product of increased filamin associations which would likely increase MSC activity. We have nearly completed a talin-cpstFRET chimera.

The data in Figure 14 was aquired at low temporal resolution (10 Hz) with respect to MSC inactivation kinetics. To determine how the mechanical response of these chimeras compares to MSC kinetics we need much higher temporal resolution. Preliminary data on the filamin cells treated with PGE2 collected

at 100 Hz shows the same general increase in stress as observed at the lower frame rate. However, we can now begin to see the time dependent changes in the stress durng the 500 ms indentation. We are incorporating timed burst excitation with sub-millisecond duration that will allow us to achieve frame rates of 500 Hz.

To complete the study on inflammatory sensitivity of the MSCs and cytoskeleton, we will test the dynamic response of actinin and filamin at higher temporal imaging resolution for PGE2 only; the strongest inflammatory agent. This data will then be combined with the MSC data in Aim 2 and published as a single manuscript. We will also try to determine the sensitivity of the spectrin-CpstFRET chimera for inclusion in the manuscript. Though the efficiency of spectrin expression has been soomewhat problematic.

Aim 4) In vivo analgesic properties of GsMTx4

This goal of this aim was to determine the potential analgesic properties of GsMTx4 for pain by in-vivo testing in rats. Initial tests preformed in the beginning of the grant period were not able to reproduce the results in the literature. However, recent PK analysis by Tonus Therapeutics (company licenced for pharmaceutical development of GsMTx4) may shed light on dosing that will achieve the peripheral tissue concentrations necessary to observe analgesic properties in a more consistent manner. We would like to point out that the Sachs lab in collaboration with Dr. Ji Li of the the Dept. of Pharmacology at the University of Buffalo have submitted a manuscript showing in vivo efficacy of GsMTx4-D in treating ischemic reperfusion injury. This paper shows suggests that there is an optimal tissue concentration for achieving the greatest cardio-protection. This may be relevant to the case of GsMTx4 use as an analgesic. Future analgesic testing will be undertaken once an new comprehesive PK/PD analysis of GsMTx4 is completed by Tonus which is planned to begin in the next several months.

Key Research Accomplishments:

Aim 1)

1) Lipid binding experiments suggest that GsMTx4 bilayer depth of penetration is optimal for inhibitory activity, and that any dispalcement from this position reduces its inhibitory activity. This goes against our previous conclusions that GsMTx4 activity is derived from its ability to enter deep binding mode.

2) GsMTx4 forms aggregates, but at concentrations above its KD for inhibiting channels suggesting this is not a factor in its inhibitory mechanism.

Aim 2)

1) Mutations to Piezo channels that lead to Xerocytosis and Arthrogryposis cause slower inactivation which effectively increases cation current in the effected cells of these disorders.

2) Fluorescent labeling of Piezo channels was achieved without disrupting channel function. Chimeric channel proteins containing roughly either the N or C terminal halves of the piezo 1 channel fused with fluorescent proteins at internal sites (instead of termini) showed that the channel gating requires both halves of the protein.

3) Inflammatory agents generally lead to increased MS current aplitude and slower inactivation rates, both of which would increase sensitivity of neuronal response to mechanical stimulation.

4) GsMtx4 effectively inhibits rapidly adapting MS currents such as those produced by Piezo channels. However, it was less effective at inhibiting slow adapting MS currents which are thought to be associated with TRPA1 channels.

5) We can observe MS currents in DRGs with using voltage sensitive membrane dyes which will significantly increase the efficiency of testing MSC activity in the future.

Aim 3)

1) Demonstrated important general concents of cpstFRET chimeras expressed in DRGs:

    a. Inflammatory agents can "increase" static and dynamic stress.

    b. Cytoskeletal elements can be differentially affected by test substances (CGS produced indentation sensitivity only in filamin).

    c. Stress on a specific cytoskeletal element responds differentially to different reagents (actinin showed sensitivity to indentation after treatment with PGE2 but not 5-HT or CGS).

    d. Stress distributions are complicated since changes in static stress do not necessarily translate into dynamic changes (PGE2 induced little change in the static stress on filamin, but caused high sensitivity to indentation stress).

2) The dynamic response of filamin, an important adaptor protein in controlling membrane mechanics, shows a large increase in stress sensitivity after treatment with PGE2. In correlation with this finding, PGE2 also produced the largest increase in MS current amplitude and decay rate.

Reportable Outcomes:

Publications

Bae, C., P.A. Gottlieb, and F. Sachs, *Human PIEZO1: removing inactivation.* Biophys J, 2013. **105**(4): p. 880-6.

Conference Abstracts:

Biophysics conference:

1) Radhakrishnan Gnanasambandam, Chilman Bae, Philip A. Gottlieb, Frederick Sachs. **Pore Properties of the Human Piezo1 Channel Based on Cation Permeation**, 2806-Pos Board B498.

2) Philip A. Gottlieb, Chilman Bae, Thomas Suchyna, Frederick Sachs. **Two Segments of the Human PIEZO1 Mechanosensitive Ion Channel CanReassemble into a Functional Unit**, 1572-Pos Board B302.

3) Radhakrishnan Gnanasambandam, Frederick Sachs, Thomas Suchyna. **Effect of Inflammatory Mediators on Cytoskeletal Stress and Endogenous Mechanosensitive Currents in Dorsal Root Ganglion Neurons**, 2807-Pos Board B499.

Grants Submitted:

DoD Clinical and Rehabilitative Medicine Neurosensory Research Award, Opportunity Number: W81XWH-13-DMRDP-CRMRP-NSRA, Sachs - PI, Suchyna and Gottlieb – CoPIs. Title: Regulation of Mechanosensitive Ion channels in Nocioceptive Neurons and the Mechanism of Action of Peptide Inhibitor GsMTx4, 9/1/2014 – 8/31/2014.

Conclusions:

We have made considerable progress this year in 1) understanding the mechanism of GsMTx4 inhibition, 2) the properties of Piezo channel inactivation, and 3) how inflammatory agents increase DRG sensitivity to mechanical stimulation. We have gone beyond functional testing of GsMTx4, and incorporated physicochemical analyses that has shed light on the mechanism of GsMTx4 interaction with membranes. This is precisely the type of information we need to design different types of MSC inhibitors, whether by increasing selelctivity for specific channel types (since it is likely different MSCs reside in different membrane domains) or by increasing potency of inhibition (mutations stabilizing its depth of penetration will likely increase potency).

We have shown that naturally occurring mutations in Piezo 1 channels that cause disease in humans are associated with reduced inactivation of the channel and not the pore. This empahasizes the importance of understanding the factors that control this inactivation of the channel. Inactivation modulation has also been associated with hypersensitivity of peripheral somatic neurons to mechanical stimulation. We have also determined sites in Piezo 1 amenable to flourescent labeling which will aide us in our studies of the channel. In so doing we have learned that elements necessary for channel conduction of ions and/or gating reside in both halves (N and C termini).

We have developed considerable expertise in expression of exogenous proteins in DRG neurons and in monitoring their mechanotransducers (MSCs) and the mechanical controlling agents (cytoskeleton). We have shown that in general, natural inflammtory agents, or synthetic agents that elicit the inflammatory pathways, increase MSC current amplitude and slow inactivation. It was also shown that the cytoskeleton reacts to these same agents by absorbing greater amounts of stress. Though not all inflammatory agents were equivalent in potency of eliciting mechanical sensitivity. Filamin, an important regulator of cortical remodeling, was shown to be particularly sensitive to dynamic stress changes of the magnitude that activate MSCs.

The progress in the last year has strongly positioned us to advance the understanding of mechanical pain sensation, and provided clues to therapeutic treatment of peripheral pain.

References:

1. Chen, R. and S.H. Chung, *Effect of gating modifier toxins on membrane thickness: implications for toxin effect on gramicidin and mechanosensitive channels.* Toxins (Basel), 2013. **5**(2): p. 456-71.
2. Hao, J. and P. Delmas, *Multiple desensitization mechanisms of mechanotransducer channels shape firing of mechanosensory neurons.* J Neurosci, 2010. **30**(40): p. 13384-95.
3. Andolfo, I., et al., *Multiple clinical forms of dehydrated hereditary stomatocytosis arise from mutations in PIEZO1.* Blood, 2013. **121**(19): p. 3925-35, S1-12.
4. Albuisson, J., et al., *Dehydrated hereditary stomatocytosis linked to gain-of-function mutations in mechanically activated PIEZO1 ion channels.* Nat Commun, 2013. **4**: p. 1884.
5. Coste, B., et al., *Piezo1 and Piezo2 are essential components of distinct mechanically activated cation channels.* Science, 2010. **330**(6000): p. 55-60.
6. Poole, K., et al., *Tuning Piezo ion channels to detect molecular-scale movements relevant for fine touch.* Nat Commun, 2014. **5**: p. 3520.
7. Bae, C., P.A. Gottlieb, and F. Sachs, *Human PIEZO1: removing inactivation.* Biophys J, 2013. **105**(4): p. 880-6.
8. Michel, K., et al., *Fast calcium and voltage-sensitive dye imaging in enteric neurones reveal calcium peaks associated with single action potential discharge.* J Physiol, 2011. **589**(Pt 24): p. 5941-7.

Human PIEZO1: Removing Inactivation

Chilman Bae, Philip A. Gottlieb, and Frederick Sachs*
Department of Physiology and Biophysics and The Center for Single Molecule Biophysics, State University of New York at Buffalo, Buffalo, New York

ABSTRACT PIEZO1 is an inactivating eukaryotic cation-selective mechanosensitive ion channel. Two sites have been located in the channel that when individually mutated lead to xerocytotic anemia by slowing inactivation. By introducing mutations at two sites, one associated with xerocytosis and the other artificial, we were able to remove inactivation. The double mutant (DhPIEZO1) has a substitution of arginine for methionine (M2225R) and lysine for arginine (R2456K). The loss of inactivation was accompanied by ~30-mmHg shift of the activation curve to lower pressures and slower rates of deactivation. The slope sensitivity of gating was the same for wild-type and mutants, indicating that the dimensional changes between the closed and open state are unaffected by the mutations. The unitary channel conductance was unchanged by mutations, so these sites are not associated with pore. DhPIEZO1 was reversibly inhibited by the peptide GsMTx4 that acted as a gating modifier. The channel kinetics were solved using complex stimulus waveforms and the data fit to a three-state loop in detailed balance. The reaction had two pressure-dependent rates, *closed* to *open* and *inactivated* to *closed*. Pressure sensitivity of the opening rate with no sensitivity of the closing rate means that the energy barrier between them is located near the open state. Mutant cycle analysis of inactivation showed that the two sites interacted strongly, even though they are postulated to be on opposite sides of the membrane.

INTRODUCTION

PIEZO1 is a eukaryotic mechanosensitive cation-selective channel (1–3) of ~2500 amino acids containing 30 putative transmembrane domains (1,4,5). It has electrophysiological properties similar to many endogenous cationic mechanosensitive ion channels (MSCs), with a reversal potential around 0 mV, voltage-dependent inactivation, and inhibition by the peptide GsMTx4 (6,7). PIEZO1 forms homotetrameric aggregates (2), but it is not known whether the pore is located in the monomers or at the interfaces.

The channel is sensitive to its physical environment because the gating kinetics are not identical in patch and whole-cell recordings (8). The channels appear to exist in physical domains that can be fractured at stresses below the lytic strength of the bilayer (7). The domains might consist of clusters of channels, lipid phases, or cytoskeletal corrals (9).

Mutations (M2225R and R2456H) that produce human hereditary xerocytosis (an autosomal dominant anemia) have slower inactivation rates than wild-type (WT) (7,10,11) and an increased latency to activation (7). The longer open times due to slow inactivation will produce the larger cation fluxes that seem to be associated with hereditary xerocytosis (7,10,11), but longer latencies will reduce the flux for transient stimulations such as passage through capillaries. The mutations do not seem to act via changes in residue charge because the conservative mutation of arginine to lysine at position 2456 slowed inactivation.

A double mutant, DhPIEZO1, substitutes an arginine for a methionine at position 2225 (M2225R), which is associated with hereditary xerocytosis, and a lysine for an arginine at position 2456 (R2456K), which we created. The single-site mutants inactivated slower than WT (7), but the double mutant did not inactivate at all. To examine whether the two sites interacted to produce the loss of inactivation, we did a mutant cycle analysis and estimated the free energy for inactivation for WT, single-site mutants, and the double mutant. The analysis shows a strong interaction.

Other properties of DhPIEZO1 were similar to WT, including the near-zero Na/K reversal potential and inhibition by GsMTx4. The gating curves (the Boltzmann relationship of open probability vs. pressure) showed that the dimensional change between closed and open states was similar to WT, although the midpoint of the gating curve was shifted to lower pressures. The channel kinetics of all channel types, even for complex stimuli, could be fit with a simple three-state closed loop model (closed–open–inactivated) in detailed balance with only two pressure-dependent rates.

MATERIALS AND METHODS

The bath solution contained (in mM) 150 NaCl, 5 KCl, 1 $MgCl_2$, 2.5 $CaCl_2$, 10 HEPES, pH 7.4 (adjusted with NaOH). The pipette solution contained (in mM) 150 CsCl, 10 HEPES, 5.0 EGTA, 1.0 $MgCl_2$, 1.0 $CaCl_2$, pH 7.3 (adjusted with CsOH), or 150 KCl, 10 HEPES, 0.25 EGTA, 0.5 $MgCl_2$, pH 7.3 (adjusted with KOH). Patch pipettes had resistances of 2–5 MΩ. The mechanical stimulus for patches was pipette suction for cell-attached patches and pipette pressure for outside-out patches. All pressure stimuli were applied by a high-speed pressure clamp (ALA Scientific Instruments, Farmingdale, NY). Whole-cell and patch-clamp currents were recorded using an Axopatch 200B amplifier (Axon Instruments), sampled at 10 kHz,

Submitted May 8, 2013, and accepted for publication July 16, 2013.
*Correspondence: Sachs@buffalo.edu
Editor: Michael Pusch

0006-3495/13/08/0880/7 $2.00
http://dx.doi.org/10.1016/j.bpj.2013.07.019

and low pass filtered at 1 kHz. Patch capacitance and conductance were measured as previously described (12,13) using an EG&G 5208 two-phase lock-in analyzer (Oak Ridge, TN).

The dose–response data were fit to a Boltzmann relationship, and when we had two different types of channels in a patch, the data were fit to the sum of two Boltzmann functions:

$$I = A + Im_1 \times \left[1 - \frac{1}{1 + e^{(q_1 \times (p_1 - p))}}\right] + Im_2 \times \left[1 - \frac{1}{1 + e^{(q_2 \times (p_2 - p))}}\right],$$

where Im_i is the maximum available current for channel type i, p_i is the pressure at half activation, q_i is the slope sensitivity, and A is an instrumental offset.

Whole-cell mechanical stimulation used a fire-polished glass pipette (diameter of 2–4 μm) positioned at an angle of 30° with respect to the cover glass to press on voltage clamped cells. The probe was coarsely positioned ~15 μm above the cell; from that position, we applied a trapezoidal downward waveform with a piezoelectric stage (P-280.20 XYZ NanoPositioner, Physik Instrumente). The indentation depth with 40-nm resolution was controlled using LabVIEW. The probe velocity was 0.15 μm/ms during transitions, and the indentation was held constant for 300 ms. Currents were generally recorded at a holding potential of −60 mV at room temperature. Hypotonic swelling was initiated by adding distilled water in equal volume to the bath solution.

To compute the channel kinetics, we applied a series of square suction pulses with variable off times (3.0, 2.0, 1.0, 0.5, 0.25, 0.1 s, and the reverse) usually in the cell-attached mode. These multichannel currents were analyzed using the MAC routine of QuB software (www.qub.buffalo.edu).

HEK-293 cells were transfected with 750 ng cDNA using Fugene (Roche Diagnostic, Indianapolis, IN) according to manufacturer's specification and transfected cells were tested 24–48 h later. The peptide GsMTx4 was synthesized, folded, and purified as previously described (14) and applied through an ALA perfusion system. Data acquisition and stimulation were all controlled by QUBIO software (www.qub.buffalo.edu).

RESULTS

Whole-cell data

At a given membrane potential, the currents increased with indentation depth (Fig. 1, *A* and *B*). In contrast to the WT channel (Fig. 1 *A*) and the single-site mutants (M2225R and R2456K) (7) that displayed faster or slower inactivation, respectively, DhPIEZO1 produced a steady-state current with sustained indentation (Fig. 1 *B*). DhPIEZO1 currents are mechanically sensitive, have no inactivation, and relative to WT, the channels are sensitized toward the open state. The fact that the DhPIEZO1 current persisted in steady state suggests that in the domains containing the channels there is no time-dependent adaptation of the local stimulus (13,15).

Osmotic pressure is often applied as an alternative stimulus to direct mechanical stimulation, but much of the osmotic stress is contained in the deep cytoskeleton, not the bilayer (16), so osmotic pressure is not an equivalent stimulus to direct stress. Nonetheless, we have found that hypoosmotic

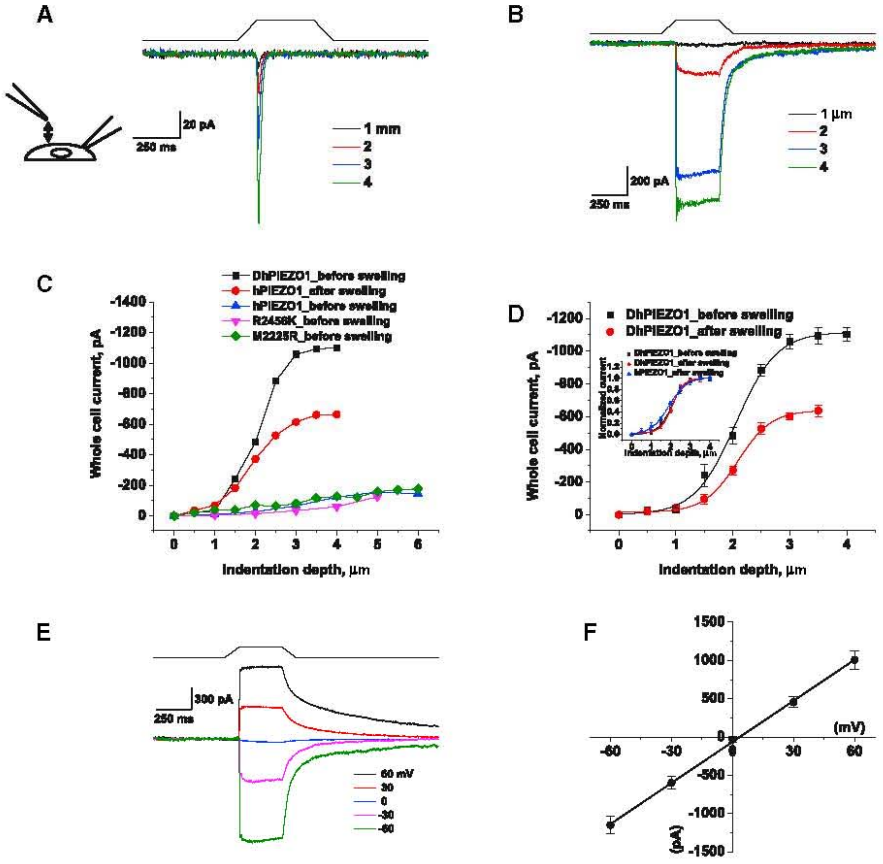

FIGURE 1 DhPIEZO1 does not inactivate. *(A)* Whole-cell currents of WT hPIEZO1 rapidly inactivate. *(B)* Whole-cell currents of DhPIEZO1 as a function of indentation depth showed no inactivation. Note the slow rate of deactivation after the stimulus is removed. *(C)* WT channels are sensitive to hypotonic swelling. Prior to swelling, there was less current for the same incremental indentation than after swelling. Also shown is the response of DhPIEZO1 prior to swelling. *(D)* Comparison of DhPIEZO1 responses before and after hypotonic swelling with 50% osmolarity. The inset shows the same data normalized. The sensitivity to indentation is similar, suggesting that the channels are already near a saturated level of stress in the resting state. *(E)* Deactivation is extremely slow and voltage independent. Deactivation for this channel may represent the kinetics of domain reformation rather than channel kinetics. *(F)* The I/V curve of peak currents shows a reversal potential near 0 mV for DhPIEZO1, indicating that the mutations do not affect the pore.

pressure increased the sensitivity of WT hPIEZO (Fig. 1 *C*) similar to results reported for the mouse channel (mPIEZO1) (8). In contrast, DhPIEZO1 proved insensitive to cell swelling, even when 50% distilled water was added to the bath (Fig. 1, *C* and *D*). This implies that the resting stress in the channel (prestress) is nearly saturated.

Because the rate of inactivation in WT and single-site mutants is voltage sensitive (1,6–8), we examined DhPIEZO1 from −60 to +60 mV. Fig. 1 *E* shows that the rate of inactivation was close to zero at all potentials. DhPIEZO1 *deactivation* was extremely slow relative to that of single-site mutants and WT, suggesting a structural correlation between inactivation and deactivation. All channel types had a similar ionic selectivity with a Na/K reversal potential of ~0 mV (Fig. 1 *F*), so that the mutations are not likely to be located near the pore.

Patch data

Cell-attached patches of DhPIEZO1 are mechanically sensitive and showed no inactivation, but had an increased latency for activation. The steady-state gating curve of DhPIEZO1 (Fig. 2 *A*) in patches was well fit by a Boltzmann function of $I = A + I_{max} \times (1 - 1/(1 + \exp(q \times (p - p_{1/2}))))$, where I_{max} is the maximum available current, p is the pressure, $p_{1/2}$ is the pressure at half activation, and q is the slope sensitivity to pressure. For DhPIEZO1, $p_{1/2} = -9.9 \pm 0.6$ mmHg, and the slope sensitivity, q, was 0.15 ± 0.01 mmHg^{-1} (*SD*, $n = 12$). For WT, the midpoint $p_{1/2} = -38.1 \pm 0.4$ mmHg and $q = 0.15 \pm 0.01$ mmHg^{-1} (*SD*, $n = 18$) comparable to previously measured values (7). The q-values of all channel types were the same, implying that the dimensional changes between the closed and open states are the same. The decrease in $p_{1/2}$ with constant q implies that the mutations added resting stress to the structure (prestress), favoring the open state. In terms of energy, the data indicate that the mutations decreased the energy of the open state while maintaining the difference in energy between the closed state and the barrier peak.

To calibrate the absolute sensitivity of DhPIEZO1, we cotransfected cells with a eukaryotic-expressing bacterial MSC called MscL that has been calibrated in bilayers (17,18). These cotransfection data were fit to the sum of two Boltzmanns, simultaneously solving for q and $p_{1/2}$ for both channels in the same patch (see *inset* in Fig. 2 *B*). The ratio of slope sensitivities for DhPIEZO1 to MscL was 0.98 ($n = 5$), so that both channels had similar dimensional changes between the closed and open states, equivalent to 20 nm^2 of in-plane area (17,19).

DhPIEZO1 was highly sensitive to the absolute level of pressure as a result of the leftward shift of the dose–response curve for pressure. A typical single-channel recording (Fig. 3 *A*) shows that a 3-mmHg change of suction, from −12 to −15 mmHg, resulted in a significant change in the number of active channels. These data were fit to a

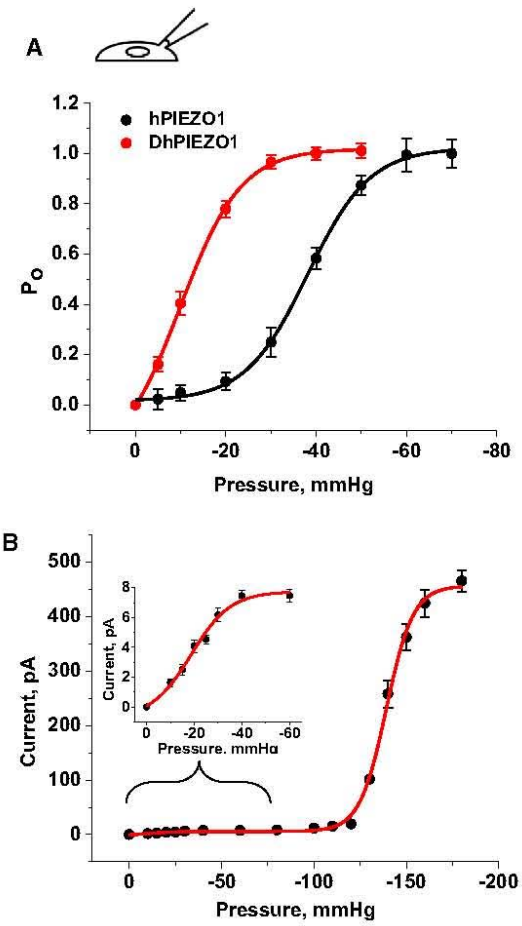

FIGURE 2 *(A)* The gating curve as a function of pressure fit to a Boltzmann. $p_{1/2}$ and the slope sensitivity q are indicated in the table. q is a measure of the dimensional change between closed and open states. q is the same for DhPIEZO1 ($n = 12$), WT ($n = 18$), and the single-site mutants, implying that the mutations have no effect on the key activation processes. However, $p_{1/2}$ was left-shifted relative to WT, representing a change in the intrinsic stress of the channel environment favoring the opening state. *(B)* To calibrate the absolute stress sensitivity, we cotransfected cells with bacterial MscL (7) and DhPIEZO1. Fit to a sum of two Boltzmanns, the slope sensitivities of both channels were nearly identical ($n = 5$), meaning that the dimensional changes of both channels are similar and also similar to WT and single-site mutants. The dimensional changes are equivalent to an in-plane area change of 20 nm^2.The inset shows an expansion of the region containing DhPIEZO1's response.

two-state model with a pressure-dependent opening rate and the same slope sensitivity as WT (Fig. 3 *A*). This extreme sensitivity is interesting considering that the resting patch is already under a large resting tension on the order of 1 to 2 mN/m because of adhesion of the gigaseal (15,20,21). Consistent with the higher absolute sensitivity of DhPIEZO1, we observed an increase in spontaneous openings (Fig. 3 *B*).

In contrast to WT channels that had no measurable latency for activation, DhPIEZO1 had a pronounced latency of ~250–350 ms followed by sudden activation (Fig. 3, *B* and *C*). The kinetics of the activation cannot be fit by simply adding more closed states prior to opening. We have proposed that the observed latency represents the time required

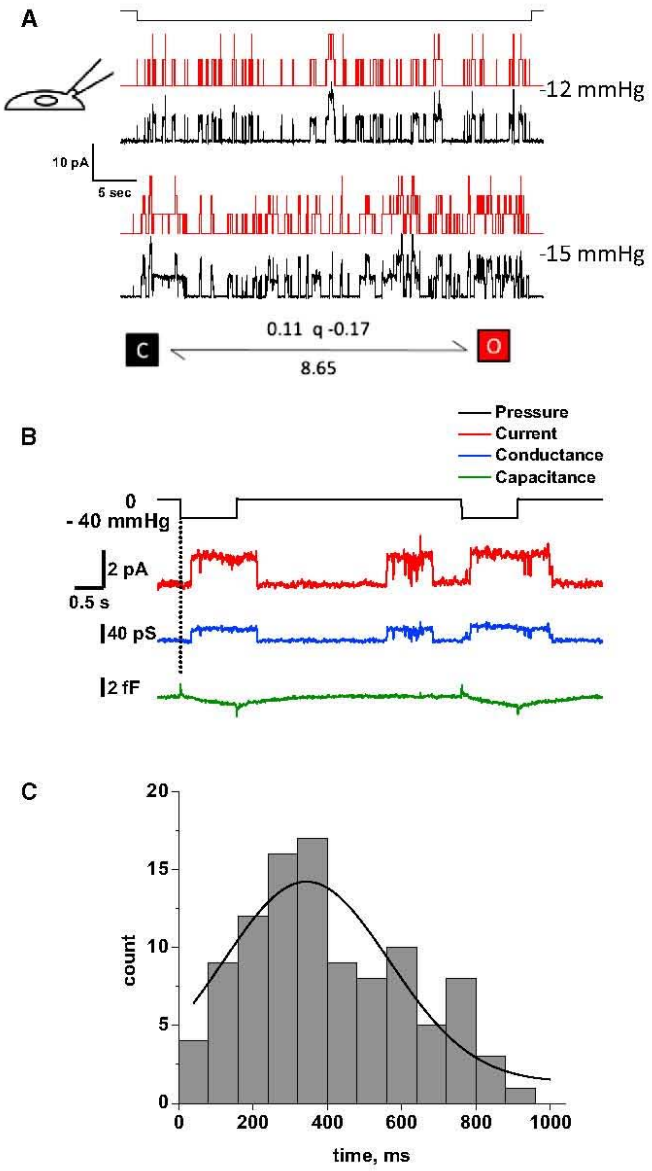

FIGURE 3 *(A)* DhPIEZO1 single-channel currents show high pressure sensitivity because of the left shift in the gating curve. The current trace is shown in black and the theoretical fit is in red. With a change of only 3 mmHg, there is a significant increase in the number of open channels. The kinetics are well fit by a two-state model with only the activation rate being pressure dependent. *(B)* Single-channel currents of DhPIEZO1 have a pronounced latency for activation, and this occurs with no significant change in patch capacitance, suggesting that the latency does not arise from large changes in the patch structure. The capacitance measuring noise level was 0.12 fF RMS, equivalent to ~0.012 μm^2 (assuming a specific capacitance of 1 $\mu F/cm^2$, or 10 $fF/\mu m^2$). Note the spontaneous (background) channel openings of DhPIEZO1 during the recording that is a result of its higher absolute sensitivity and tension from the gigaseal. *(C)* The distribution of latencies fit to a Gaussian gives a mean latency of 344 $\pm$ 133 ms. We attribute these latencies to the time required for domain fracture under stress.

for the domain boundary to fracture and to change the stress on the channels (7). A change in the domain, such as fracturing a caveolus, might produce a change in area and hence a change in patch impedance. We tried to measure such a change (12,13) but we observed none (Fig. 3 *B*). The measurement noise level placed an upper limit on any area change to < 0.01 μm^2. This suggests that the domain fracture probably did not involve opening of a vesicular structure such as a caveolus.

Inhibition by GsMTx4

PIEZO1 currents are reversibly inhibited by the D-enantiomer of GsMTx4, a specific inhibitor of cationic MSCs (6,22). The lower graph of Fig. 4 *A* shows whole-cell peak

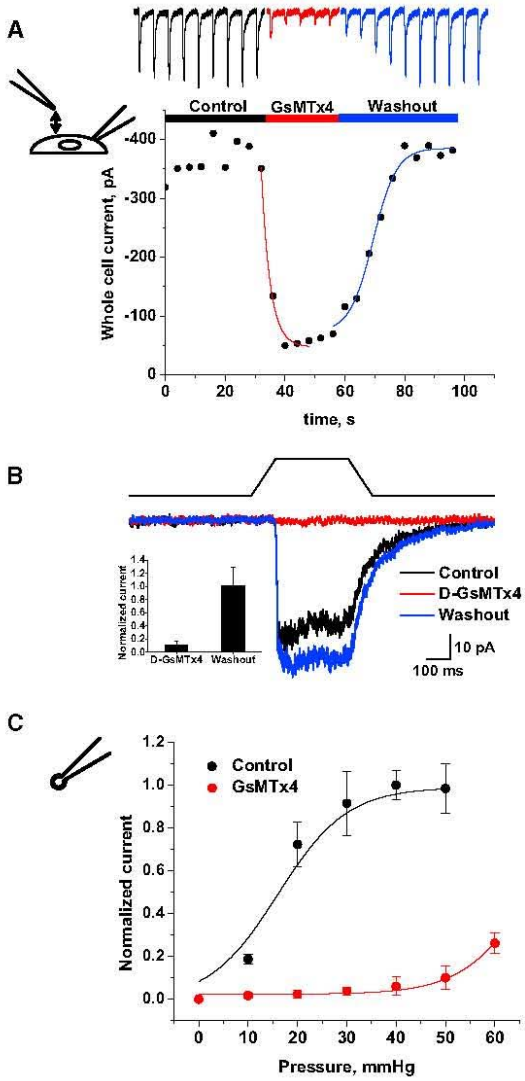

FIGURE 4 DhPIEZO1 channels in whole-cell patches were reversibly inhibited by 10 μM extracellular D-GsMTx4. *(A)* By fitting exponentials, we extracted a mean association time constant of 3.0 $\pm$ 0.6 s and a mean dissociation time constant of 13.4 $\pm$ 0.8 s ($n = 4$). The estimated association and dissociation rates are 2.6×10^4 M^{-1} s^{-1} and 0.08 s^{-1}, respectively, and the equilibrium constant calculated from the ratio is K_D ~3 μM. *(B)* D-GsMTx4 inhibition of DhPIEZO1 in the absence of inactivation. This suggests that the mechanism of action of D-GsMTx4 does not involve inactivation domains. The bar graph *(inset)* shows the average peak currents $\pm$ *SD* ($n = 3$) illustrated in Fig. 4 *B*. *(C)* The dose–response relationship shifts to higher stress with GsMTx4, as expected for a gating modifier (12).

currents as a function of time from GsMTx4 exposure through washout. From single exponential fits, the association time constant was 3.0 ± 0.63 s and the dissociation time constant was 13.4 ± 0.76 s. The ratio gives an equilibrium affinity of ~3 μm. Fig. 4 *B* shows that D-GsMTx4 inhibition occurs in the absence of inactivation so that the peptide does not seem to interact with the inactivation domain(s) of the channel. At −60 mV, 10 μM GsMTx4 caused an 89% reduction in peak current (Fig. 4 *B*). In outside-out patches (Fig. 4 *C*), the inhibition was >90%. GsMTx4 is a gating modifier acting on closed channels (6), and we estimated its efficacy to be equivalent to ~60 mmHg by the increase of suction required to obtain equal channel activity with and without GsMTx4.

Channel kinetics: Cell-attached patches

We stimulated the patch with a series of square suction pulses with varying time intervals between them (typically 3.0, 2.0, 1.0, 0.5, 0.25, 0.1 s, and the reverse). The response to the entire sequence could be fit using the MAC routine of QuB (www.qub.buffalo.edu). This nonstationary approach has many advantages over traditional single- or double-step analyses in that the responses need not reach equilibrium before the next pulse is applied. Furthermore, the fit is a global optimum for the entire sequence (i.e., the series is treated as a single stimulus; see Fig. 5 *A*).

DhPIEZO1 kinetics were fit with a simple three-state loop model (closed, open, and inactivated) in detailed balance (at all stimuli). To simplify comparison of the kinetics to WT and single-site mutations that required three states, we fit the DhPIEZO1 kinetics to the three-state model even though it had no inactivation. Detailed balance in a loop requires a minimum of two pressure-dependent rates, and we found we could satisfy that constraint with a pressure-dependent opening rate and inactivated-closed rate (Fig. 5 *B*). One of the most striking results of the kinetic analysis was that all channel types had identical slope sensitivities, q = 0.15 ± 0.005 $mmHg^{-1}$ (Fig. 5 *B*) so that the conformational change between the closed and open states of all channels was identical. Furthermore, all the channels had to be in domains with similar local stress. The preexponential coefficients of the activation rates were 10×10^{-3} s^{-1}, 4.62×10^{-3} s^{-1}, 6.13×10^{-3} s^{-1}, and 3.28×10^{-3} s^{-1} in hPIEZO1, M2225, R2456K, and DhPIEZO1, respectively, at −60mV. The mutations had little or no effect on the

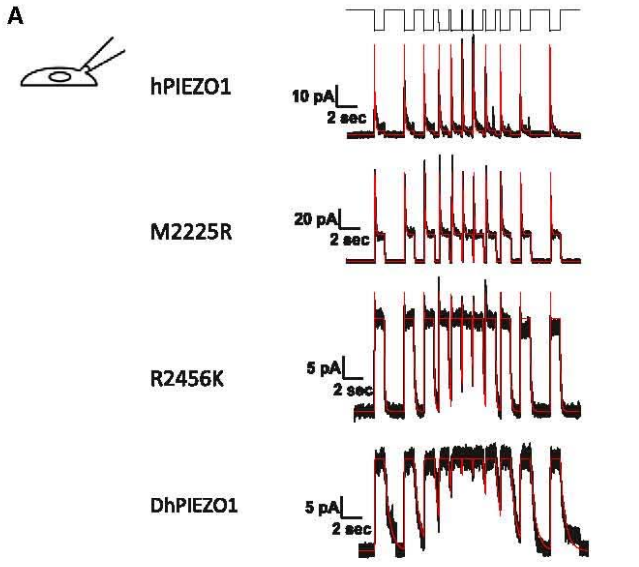

st1 → st2		hPIEZO1	M2225R	R2456K	DhPIEZO1
C	O	0.01 q -0.16	4.62e-3 q -0.15	6.13e-3 q -0.15	3.28e-3 q -0.15
O	C	1.12	1.45	8.86	2.06
O	I	8.59	12.19	2.84	5.40E-04
I	O	1.19	4.40	115.1	141.46
I	C	73.77 q 0.16	153.40 q 0.15	4408.20 q 0.15	1888.80 q 0.15
C	I	3.28	1.35	0.08	1.22E-05

FIGURE 5 Channel kinetics. *(A)* Multichannel currents for different types of channels. The stimulus was a series of square pressure pulses applied with varying off intervals (typically 3.0, 2.0, 1.0, 0.5, 0.25, 0.1 s, and the reverse, *top trace*). Pressure pulses were 0 to −70 mmHg for HPIEZO1, 2555R PIEZO1, and 2456K PIEZO. For DhPIEZO1, they were 0 to −40 mmHg. The data trace is in black and the QuB fit in red. Notice how hPIEZO1 effectively summed currents from the applied stresses at short off-times of the stimulus. However, the mutant M2225R tended to accumulate inactivation in the same part of the stimulus (lower peaks at shortest resting intervals), but this can be accounted for simply by a change in the rate constants and requires no additional states. The kinetic parameters that characterize the behavior of all channels are presented in *(B)*. *(B)* Tabulation of the quantified kinetics with the three-state loop in detailed balance. The states are named C =closed state, O = open state, and I = inactivated state. Although DhPIEZO1 does not appear to have an inactivated state, we included it for consistency to better compare the models. The pressure dependence for all channel types is contained in the opening rate and the inactivated-closed rate. The pressure sensitivity of the rates is indicated by the parameter q [$mmHg^{-1}$]. q was consistent across all types of channels at ~0.15 so that the conformation associated with opening in all channel types is identical. The DhPIEZO1 trace ends with a jump that is probably closure of the last open channel.

0-mmHg opening rates (the preexponential coefficients). Because the preexponential term contains the entropy of activation, we infer that the mutations also did not change that component of the free energy.

Inactivation is fast in hPIEZO1, M2225R, and R2456K ($12.7\ s^{-1}$, $9.8\ s^{-1}$, $12.4\ s^{-1}$ at −60 mV, respectively), and DhPIEZO1 effectively did not inactivate ($< 1.6 \times 10^{-6}\ s^{-1}$ at −60 mV). When we examined deactivation, hPIEZO1 and M2225R were faster than the pressure clamp's response time, but R2456K was slow enough to measure ($6.2\ s^{-1}$), and DhPIEZO1 was even slower ($2.4\ s^{-1}$). Deactivation represents the process of going from open to closed and is characterized by the energy difference between the open state and the energy barrier between the open and closed state. If the change in deactivation rate was due to a change in barrier height, we would expect that the slope sensitivity for opening, q, would also change, but it did not, so the change in deactivation rate appears to represent changes in the open state energy. Slow deactivation of DhPIEZO1 may represent reforming of the domain, the inverse of fracturing. The C-terminal domain, where the mutations are located, is presumably involved in domain creation (7).

To explore whether the two mutation sites were independent, we did a mutant cycle analysis of inactivation (23). If the two sites were independent, the free energy difference for inactivation of DhPIEZO1 should be the sum of the energies of the single mutants. However, the data showed that the energy of the dual mutant is much larger than the sum of the two single mutant energies, so they must be interacting. The basic calculation is as follows, where ΔG_i is the free energy with mutation of residue i, and $\Delta\Delta G_i$ is the free energy changes with mutation of residue i.

$$\Delta\Delta G_{2225} = \Delta G_{2225} - \Delta G_{WT}.$$
$$\Delta\Delta G_{2456} = \Delta G_{2456} - \Delta G_{WT}.$$
$$\Delta\Delta G_{DhPIEZO1} = \Delta G_{DhPIEZO1} - \Delta G_{WT}.$$

$$\begin{aligned}\Delta G &= \Delta\Delta G_{DhPIEZO1} - (\Delta\Delta G_{2225} + \Delta\Delta G_{2456}) \\ &= \Delta G_{DhPIEZO1} + \Delta G_{WT} - \Delta G_{2225} - \Delta G_{2456} \\ &= -k_BT \times \left[\ln\left(\frac{5.4 \times 10^{-4}}{141.46}\right) + \ln\left(\frac{8.59}{1.19}\right)\right. \\ &\quad \left. - \ln\left(\frac{12.19}{4.40}\right) - \ln\left(\frac{2.84}{115.10}\right)\right] \\ &= 7.82\ k_BT.\end{aligned}$$

The difference of free energy $\Delta G = 7.82\ k_BT$ shows that the sites are not independent despite on apparently opposites sides of the bilayer (7).

DISCUSSION

A striking feature of activation is that the slope sensitivity q was identical for all channel types. This means that the energy between the closed and open states was identical. Perhaps even more surprising is that this also implies that the local stresses sensed by the channel were identical: The domains were similar enough that the internal stresses were the same. The free energy of gating is well approximated by $\Delta G = T\Delta A$, where T is the local tension and ΔA is the change of in-plane area so that a change in T will produce a change in ΔG. The data on DhPIEZO1 also show that activation is effectively uncoupled from inactivation.

The kinetics of all mutants could be fit with the three-state loop model with the same two pressure-dependent rates so that the mutations did not appear to introduce any new states (Fig. 5). The fact that the kinetics of all the channels could be fit with a pressure-sensitive opening rate and a pressure-independent closing (deactivation) rate means that the energy barrier between the states is located close to the open state.

Because the slope sensitivity for activation was constant across all mutations, slowing the inactivation rate increases the channel open time for a transient stimulus. We have previously shown that PIEZO1 inactivates and does not adapt (8). To slow inactivation, one elevates the energy barrier between the open and inactivated states. But because the slope sensitivity for activation, q, was unchanged among the mutants, the difference in energy between the closed state and the barrier peak has to remain constant. Thus, the slowing of inactivation appears to represent a lowering of the energy of the open state.

The fact that the mutations caused changes in both the inactivation rate and the deactivation rate suggests that the two processes are coupled. A channel with fast inactivation, such as the WT, also has fast deactivation. When inactivation is slow (DhPIEZO1), then deactivation is slow. We previously suggested that inactivation may reflect an increased interaction between monomers to form clusters (domains) and that the regions of the channel altered by the mutations are also involved in intermonomer binding (7). DhPIEZO1 channels with no inactivation and slow deactivation may exist in loose, easily fractured clusters. The DhPIEZO1 kinetic behavior is quite similar to what we observed with the removal of the C-terminal domain (7).

Mutant cycle analysis of inactivation using WT, single-site mutants, and DhPIEZO1 (23) showed that the two sites interacted with ~8 k_BT of energy (Fig. 6). What is the mechanism of coupling? It could be part of a common flexible region of the channel or possibly affect binding to the cytoskeleton and extracellular matrix, but that is doubtful given that we have previously demonstrated that disruptors of the cytoskeleton, such as CytochalasinD, disrupt whole-cell currents. However, we know that the channels are still present because patches from those cells show functional channels. The cytoskeletal disruptors probably do not affect the channel itself but more likely the mechanical pathways that affect the local distribution of stress (8). A lack of interaction with cytoskeletal proteins is supported by

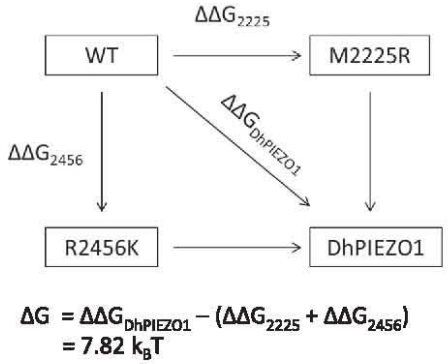

FIGURE 6 Mutant cycle analysis. The energy difference between open and inactivated states for WT, single-site mutants, and DhPIEZO1. The free energy change in DhPIEZO1 ($\Delta\Delta G_{\mathrm{DhPIEZO1}}$) is larger than the sum of free energy changes for the two single mutants by ~8 k_BT, showing that the sites are not independent but exhibit positive cooperativity.

mass-spectrum analysis of mPIEZO1 that shows no additional proteins bound to the purified channel (2).

DhPIEZO1 may be a good candidate for developing a high throughput screen for inhibitors of PIEZOs. Given that it lacks inactivation, a persistent mechanical stimulus to DhPIEZO1 will induce a persistent calcium influx, making the assay insensitive to variations in the rates of inactivation. Furthermore, inhibition by the specific reagent GsMTx4 is a positive control.

This work was supported by the National Institutes of Health, Department of Defense, and the Children's Guild of Buffalo. We are grateful to Joanne Pazik and Lynn Zeigler for expert technical assistance on the molecular biology and Julia Doerner from David Clapham's laboratory for sharing the eukaryotic vector for expression of the MscL.

REFERENCES

1. Coste, B., J. Mathur, ..., A. Patapoutian. 2010. Piezo1 and Piezo2 are essential components of distinct mechanically activated cation channels. *Science.* 330:55–60.
2. Coste, B., B. Xiao, ..., A. Patapoutian. 2012. Piezo proteins are pore-forming subunits of mechanically activated channels. *Nature.* 483:176–181.
3. Kim, S. E., B. Coste, ..., A. Patapoutian. 2012. The role of Drosophila Piezo in mechanical nociception. *Nature.* 483:209–212.
4. Gottlieb, P. A., and F. Sachs. 2012. Piezo1: properties of a cation selective mechanical channel. *Channels (Austin).* 6:214–219.
5. Nilius, B., and E. Honoré. 2012. Sensing pressure with ion channels. *Trends Neurosci.* 35:477–486.
6. Bae, C., F. Sachs, and P. A. Gottlieb. 2011. The mechanosensitive ion channel Piezo1 is inhibited by the peptide GsMTx4. *Biochemistry.* 50:6295–6300.
7. Bae, C., R. Gnanasambandam, ..., P. A. Gottlieb. 2013. Xerocytosis is caused by mutations that alter the kinetics of the mechanosensitive channel PIEZO1. *Proc. Natl. Acad. Sci. USA.* 110:E1162–E1168.
8. Gottlieb, P. A., C. Bae, and F. Sachs. 2012. Gating the mechanical channel Piezo1: a comparison between whole-cell and patch recording. *Channels (Austin).* 6:282–289.
9. Rawicz, W., B. A. Smith, ..., E. Evans. 2008. Elasticity, strength, and water permeability of bilayers that contain raft microdomain-forming lipids. *Biophys. J.* 94:4725–4736.
10. Albuisson, J., S. E. Murthy, ..., A. Patapoutian. 2013. Dehydrated hereditary stomatocytosis linked to gain-of-function mutations in mechanically activated PIEZO1 ion channels. *Nat. Commun.* 4:1884.
11. Andolfo, I., S. L. Alper, ..., A. Iolascon. 2013. Multiple clinical forms of dehydrated hereditary stomatocytosis arise from mutations in PIEZO1. *Blood.* 121:3925–3935, S1–S12.
12. Suchyna, T. M., S. R. Besch, and F. Sachs. 2004. Dynamic regulation of mechanosensitive channels: capacitance used to monitor patch tension in real time. *Phys. Biol.* 1:1–18.
13. Suchyna, T. M., and F. Sachs. 2007. Mechanosensitive channel properties and membrane mechanics in mouse dystrophic myotubes. *J. Physiol.* 581:369–387.
14. Ostrow, K. L., A. Mammoser, ..., P. A. Gottlieb. 2003. cDNA sequence and in vitro folding of GsMTx4, a specific peptide inhibitor of mechanosensitive channels. *Toxicon.* 42:263–274.
15. Suchyna, T. M., V. S. Markin, and F. Sachs. 2009. Biophysics and structure of the patch and the gigaseal. *Biophys. J.* 97:738–747.
16. Spagnoli, C., A. Beyder, ..., F. Sachs. 2008. Atomic force microscopy analysis of cell volume regulation. *Phys. Rev. E Stat. Nonlin. Soft Matter Phys.* 78:031916.
17. Chiang, C. S., A. Anishkin, and S. Sukharev. 2004. Gating of the large mechanosensitive channel in situ: estimation of the spatial scale of the transition from channel population responses. *Biophys. J.* 86:2846–2861.
18. Nomura, T., C. G. Cranfield, ..., B. Martinac. 2012. Differential effects of lipids and lyso-lipids on the mechanosensitivity of the mechanosensitive channels MscL and MscS. *Proc. Natl. Acad. Sci. USA.* 109:8770–8775.
19. Sukharev, S. I., W. J. Sigurdson, ..., F. Sachs. 1999. Energetic and spatial parameters for gating of the bacterial large conductance mechanosensitive channel, MscL. *J. Gen. Physiol.* 113:525–540.
20. Ursell, T., A. Agrawal, and R. Phillips. 2011. Lipid bilayer mechanics in a pipette with glass-bilayer adhesion. *Biophys. J.* 101:1913–1920.
21. Opsahl, L. R., and W. W. Webb. 1994. Lipid-glass adhesion in gigasealed patch-clamped membranes. *Biophys. J.* 66:75–79.
22. Bowman, C. L., P. A. Gottlieb, ..., F. Sachs. 2007. Mechanosensitive ion channels and the peptide inhibitor GsMTx-4: history, properties, mechanisms and pharmacology. *Toxicon.* 49:249–270.
23. Horovitz, A. 1996. Double-mutant cycles: a powerful tool for analyzing protein structure and function. *Fold. Des.* 1:R121–R126.